RESEARCH ARTICLE

Integrative Molecular Characterization of Malignant Pleural Mesothelioma

Julija Hmeljak[1], Francisco Sanchez-Vega[2], Katherine A. Hoadley[3], Juliann Shih[4], Chip Stewart[3], David Heiman[3], Patrick Tarpey[5], Ludmila Danilova[6], Esther Drill[7], Ewan A. Gibb[8], Reanne Bowlby[9], Rupa Kanchi[10], Hatice U. Osmanbeyoglu[11], Yoshitaka Sekido[12], Jumpei Takeshita[13], Yulia Newton[14], Kiley Graim[14], Manaswi Gupta[4], Carl M. Gay[15], Lixia Diao[10], David L. Gibbs[16], Vesteinn Thorsson[16], Lisa Iype[16], Havish Kantheti[17], David T. Severson[18], Gloria Ravegnini[19], Patrice Desmeules[20], Achim A. Jungbluth[21], William D. Travis[21], Sanja Dacic[22], Lucian R. Chirieac[23], Françoise Galateau-Sallé[24], Junya Fujimoto[25], Aliya N. Husain[26], Henrique C. Silveira[27], Valerie W. Rusch[28], Robert C. Rintoul[29], Harvey Pass[30], Hedy Kindler[31], Marjorie G. Zauderer[32], David J. Kwiatkowski[33], Raphael Bueno[18], Anne S. Tsao[15], Jenette Creaney[34], Tara Lichtenberg[35], Kristen Leraas[35], Jay Bowen[35], TCGA Research Network, Ina Felau[36], Jean Claude Zenklusen[36], Rehan Akbani[10], Andrew D. Cherniack[4], Lauren A. Byers[18], Michael S. Noble[4], Jonathan A. Fletcher[22], A. Gordon Robertson[9], Ronglai Shen[7], Hiroyuki Aburatani[13], Bruce W. Robinson[34], Peter Campbell[5], and Marc Ladanyi[1]

Downloaded from http://aacrjournals.org/clincancerres/article-pdf/21/24/5487/2175885/5487.pdf by guest on 20 August 2022

ABSTRACT Malignant pleural mesothelioma (MPM) is a highly lethal cancer of the lining of the chest cavity. To expand our understanding of MPM, we conducted a comprehensive integrated genomic study, including the most detailed analysis of *BAP1* alterations to date. We identified histology-independent molecular prognostic subsets, and defined a novel genomic subtype with *TP53* and *SETDB1* mutations and extensive loss of heterozygosity. We also report strong expression of the immune-checkpoint gene *VISTA* in epithelioid MPM, strikingly higher than in other solid cancers, with implications for the immune response to MPM and for its immunotherapy. Our findings highlight new avenues for further investigation of MPM biology and novel therapeutic options.

SIGNIFICANCE: Through a comprehensive integrated genomic study of 74 MPMs, we provide a deeper understanding of histology-independent determinants of aggressive behavior, define a novel genomic subtype with *TP53* and *SETDB1* mutations and extensive loss of heterozygosity, and discovered strong expression of the immune-checkpoint gene *VISTA* in epithelioid MPM. *Cancer Discov; 8(12); 1548–65. ©2018 AACR.*

See related commentary by Aggarwal and Albelda, p. 1508.

INTRODUCTION

Malignant pleural mesothelioma (MPM) is a cancer of the mesothelial cells lining the pleural cavity. It was rare until the widespread use of asbestos in the mid-20th century (1). Although reduction and strict regulation of asbestos use may be leading to a leveling off in new cases in Western countries, its long latency, together with continued use of asbestos in non-Western countries, ensures that MPM remains a global problem (2). MPM is almost universally lethal, with only modest survival improvements in the past decade (3), suggesting that standard treatment is reaching a therapeutic plateau. Elucidating oncogenic genomic alterations in MPM is therefore essential for therapeutic progress (4–7). Frequent copy-number loss and recurrent somatic mutations in *BAP1, NF2, CDKN2A*, and others have been identified (4–6), yet no targeted therapies exploiting these alterations have emerged.

To expand our understanding of the molecular landscape and biological subtypes of MPM, and provide insights that could lead to novel therapies, we have conducted a comprehensive, multiplatform, genomic study of 74 MPM samples, as part of The Cancer Genome Atlas (TCGA). Here, we report how these integrated analyses define prognostic subsets of MPM, characterize a new near-haploid molecular subtype, and identify novel potential therapeutic targets.

[1]Department of Pathology and Human Oncology & Pathogenesis Program, Memorial Sloan Kettering Cancer Center, New York, New York. [2]Marie-Josée and Henry R. Kravis Center for Molecular Oncology, Memorial Sloan Kettering Cancer Center, New York, New York. [3]Department of Genetics, Lineberger Comprehensive Cancer Center, University of North Carolina at Chapel Hill, Chapel Hill, North Carolina. [4]The Eli and Edythe L. Broad Institute of Massachusetts Institute of Technology and Harvard University, Cambridge, Massachusetts. [5]Cancer Genome Project, Wellcome Trust Sanger Institute, Hinxton, Cambridgeshire, UK. [6]The Sidney Kimmel Comprehensive Cancer Center at Johns Hopkins University, Baltimore, Maryland. [7]Department of Epidemiology and Biostatistics, Memorial Sloan Kettering Cancer Center, New York, New York. [8]GenomeDx Biosciences, Vancouver, British Columbia, Canada. [9]Canada's Michael Smith Genome Sciences Centre, BC Cancer Agency, Vancouver, British Columbia, Canada. [10]Department of Bioinformatics and Computational Biology, The University of Texas MD Anderson Cancer Center, Houston, Texas. [11]Computational Systems Biology, Memorial Sloan Kettering Cancer Center, New York, New York. [12]Division of Cancer Biology, Aichi Cancer Center Research Institute, Nagoya, Aichi, Japan. [13]Genome Science Division, The University of Tokyo, Tokyo, Japan. [14]Department of Biomolecular Engineering and Center for Biomolecular Science and Engineering, University of California, Santa Cruz, Santa Cruz, California. [15]Department of Thoracic Head and Neck Medical Oncology, The University of Texas MD Anderson Cancer Center, Houston, Texas. [16]Institute for Systems Biology, Seattle, Washington. [17]The University of Texas at Dallas, Richardson, Texas. [18]Division of Thoracic Surgery, The Lung Center and International Mesothelioma Program, Brigham and Women's Hospital, Boston, Massachusetts. [19]Department of Pharmacy and Biotechnology, University of Bologna, Bologna, Italy. [20]Department of Pathology, Quebec Heart and Lung Institute, Quebec, Canada. [21]Department of Pathology, Memorial Sloan Kettering Cancer Center, New York, New York. [22]Department of Pathology, University of Pittsburgh Medical Center, Pittsburgh, Pennsylvania. [23]Department of Pathology, Brigham and Women's Hospital, Boston, Massachusetts. [24]MESOPATH. Cancer Center Leon Berard, Lyon, France. [25]Department of Translational Molecular Pathology, The University of Texas MD Anderson Cancer Center, Houston, Texas. [26]Department of Pathology, University of Chicago, Chicago, Illinois. [27]Molecular Oncology Research Center, Barretos Cancer Hospital, Barretos, Sao Paulo, Brazil. [28]Department of Surgery, Memorial Sloan Kettering Cancer Center, New York, New York. [29]Department of Oncology, University of Cambridge, Cambridge, UK. [30]Department of Cardiothoracic Surgery, NYU Langone Medical Center, New York, New York. [31]Department of Medicine, Section of Hematology/Oncology, University of Chicago Medical Center and Biological Sciences, Chicago, Illinois. [32]Department of Medicine, Memorial Sloan Kettering Cancer Center, New York, New York. [33]Division of Pulmonary Medicine, Brigham and Women's Hospital, Boston, Massachusetts. [34]School of Medicine and Pharmacology, University of Western Australia, Nedlands, Australia. [35]The Research Institute at Nationwide Children's Hospital, Columbus, Ohio. [36]National Cancer Institute, Bethesda, Maryland.

Note: Supplementary data for this article are available at Cancer Discovery Online (http://cancerdiscovery.aacrjournals.org/).

Current address for J. Hmeljak: The Company of Biologists, Histon, Cambridge, UK.

J. Hmeljak and F. Sanchez-Vega share first authorship of the article.

B.W. Robinson, P. Campbell, and M. Ladanyi were co-chairs of the TCGA MPM analysis working group.

Corresponding Author: Marc Ladanyi, Memorial Sloan Kettering Cancer Center, 1275 York Avenue, New York, NY 10065. Phone: 212-639-6369; Fax: 212-717-3515; E-mail: ladanyim@mskcc.org

doi: 10.1158/2159-8290.CD-18-0804

©2018 American Association for Cancer Research.

Downloaded from http://aacrjournals.org/cancerdiscovery/article-pdf/8/12/1548/1728852/1548.pdf by guest on 20 August 2022

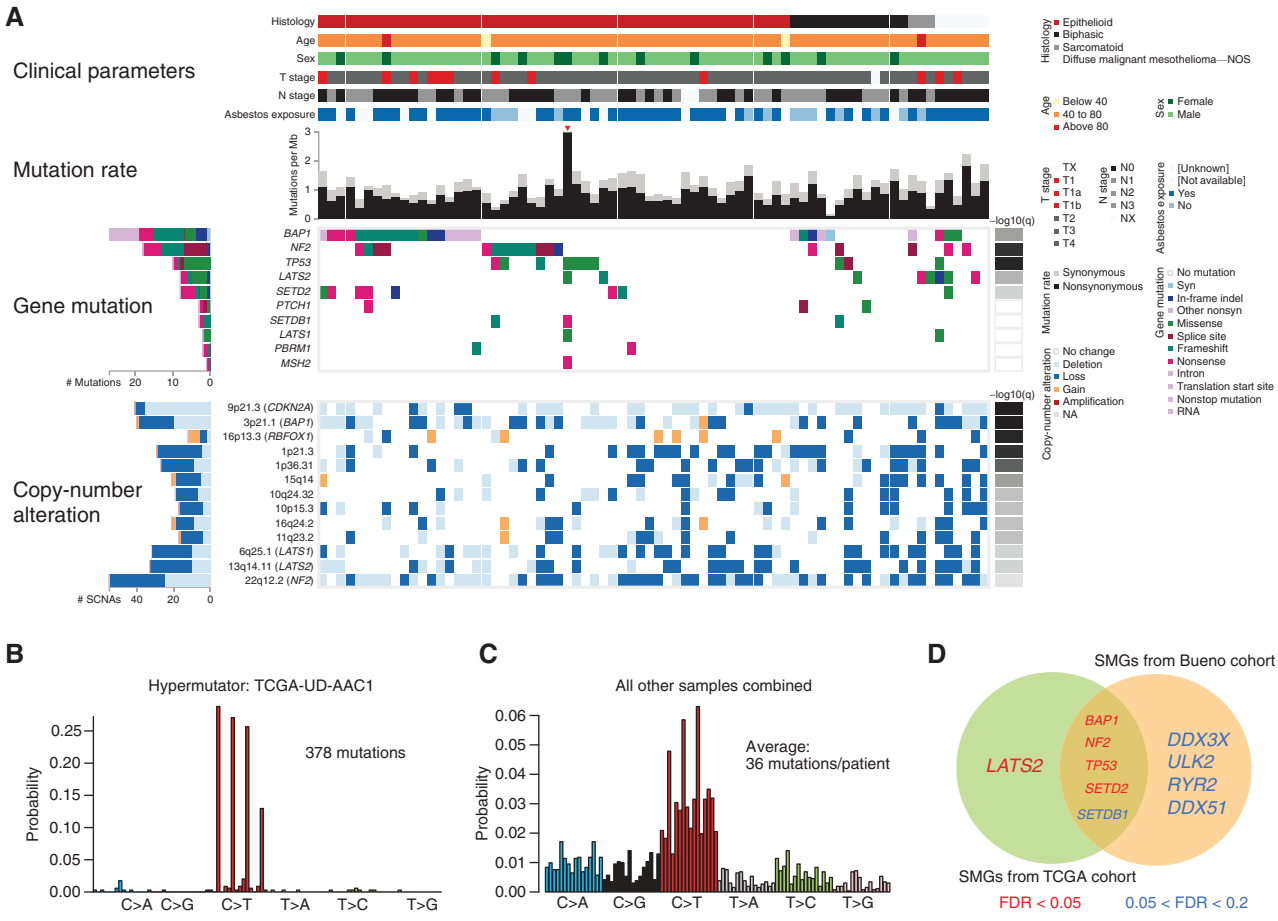

Figure 1. Genomic and clinical features of the TCGA MPM cohort. **A,** iCOMUT plot describing clinical and molecular features of the TCGA MPM cohort. Each column represents an individual case, and rows represent clinical and molecular features. Samples are grouped based on MPM histologic type. Red arrowhead indicates the hypermutated case. Copy-number alterations are defined as follows: "Deletion" is a deep loss, possibly a homozygous deletion; "Loss" is a shallow loss (possibly heterozygous deletion); "Gain" indicates a low-level gain; and "Amplification" is a high-level amplification. Individual genes shown include significantly mutated genes and selected additional genes of interest. NOS, not otherwise specified. **B,** Observed mutational spectrum of the hypermutator case (TCGA-UD-AAC1) with 375 nonsilent mutations. **C,** Observed mutational spectrum of the remaining other 73 MPM cases in the TCGA cohort (cohort average: 36 nonsilent mutations/patient). **D,** Comparison of SMGs between the present study and that of Bueno et al., 2016 (5).

RESULTS

Cohort Description

We studied 74 samples of primary MPM from patients with no prior systemic therapy. This cohort was predominantly male (82%), with a median age of 64 years, and tumors were of mostly epithelioid histology (70%), a typical profile for MPM. Asbestos exposure history was positive in 62%, negative in 18%, and unavailable or unknown in the remainder. Demographic and clinical details are provided in Supplementary Tables S1A and S1B, as well as Supplementary Fig. S1.

We performed comprehensive molecular profiling, including exome sequencing, copy-number arrays (Supplementary Fig. S2), mRNA sequencing (Supplementary Fig. S3), noncoding RNA profiling, DNA methylation (Supplementary Fig. S4), and reverse-phase protein arrays (RPPA; Supplementary Fig. S5). Methods and detailed results of individual analyses are provided in Supplementary Sections 1–13.

Landscape of Somatic Mutations and Copy-Number Alterations

Whole-exome sequencing (WES) revealed a somatic mutation rate of <2 nonsynonymous mutations per megabase in all samples except for an outlier case with a mutation rate of 8 nonsynonymous mutations per megabase (Fig. 1A). This places MPM at the low end of somatic mutation burden among cancers (8). The outlier tumor with a 10-fold higher mutation rate showed a distinctive pattern of C>T mutations occurring almost exclusively at CpG dinucleotides (Fig. 1B). This relatively hypermutated tumor harbored a homozygous nonsense mutation in *MSH2*, which would suggest that the tumor lacked mismatch-repair capacity, but the observed mutational spectrum was atypical for mismatch-repair deficiency (9). Otherwise, the observed mutational spectrum was similar across patients and lacked distinctive or novel features (Fig. 1C). Signatures of smoking- or APOBEC-induced mutagenesis were not observed. Asbestos has been proposed

Downloaded from http://aacrjournals.org/cancerdiscovery/article-pdf/8/12/1548/1728852/1548.pdf by guest on 20 August 2022

to cause genotoxicity via DNA breaks and secondary oxidative damage (10). However, the mutational spectrum and local sequence context was not significantly different between cases with or without known asbestos exposure (χ^2, $P = 0.3$); although this negative finding should be viewed with caution given the limitations of the data set, it is in agreement with prior studies (5).

We sought to identify genes mutated significantly above the background rate using MutSig2CV. Significantly mutated genes (SMG) at a false discovery rate (FDR) of <0.05 included *BAP1, NF2, TP53, LATS2,* and *SETD2*, all known cancer genes in MPM (Fig. 1A; Supplementary Table S1C). All five genes showed high rates of nonsense, frameshift, and splice-site mutations, highlighting them as targets of inactivation, consistent with their functions as tumor suppressors. Mutations in these five SMGs did not show associations with histories of asbestos exposure or smoking. For validation in an independent cohort that also used a different algorithm to define SMGs, we compared the results of our SMG analysis with the SMGs previously identified in 99 MPM exomes using the MUSIC algorithm (5) and found a strong overlap for SMGs at an FDR of <0.05 in both studies (Fig. 1D). Notably, among lower confidence SMGs (FDR < 0.15 but > 0.05), only *SETDB1*, which may define a novel subtype of MPM (discussed below), was identified in both analyses (Fig. 1D).

The somatic copy-number alteration (SCNA) landscape was characterized by frequent recurring focal and arm-level deletions, but no recurring amplifications, consistent with the notion that MPM development is driven primarily by loss of tumor suppressor genes, rather than by activation of classic oncogenic driver genes (Supplementary Section 4; Supplementary Fig. S2). Focal deletions affected several tumor suppressor genes known to be altered in MPM (5), most notably *CDKN2A* with deletions (defined as deep, likely homozygous) in 36 (49%) and losses (defined as shallow, possibly single-copy) in 5 (7%) samples. Likewise, *NF2* deletions were confirmed in 25 (34%) samples and losses in 30 (40%) samples; as many of the latter harbored mutations of the remaining allele, evidence of biallelic *NF2* inactivation was common (Fig. 1A). *CDKN2A* deletions often encompass *MTAP*, the adjacent gene on 9p21 (11), which encodes methylthioadenosine phosphorylase, whose deficiency has recently been reported to lead to reduced PRMT5 enzymatic activity and heightened sensitivity to its pharmacologic inhibition (12, 13). Codeletion of *CDKN2A* and *MTAP*, associated with low levels of mRNA expression of both genes, was observed in 20 cases (Supplementary Fig. S2). Although no correlation with overall survival was observed for *BAP1* status, loss of *CDKN2A* was strongly associated with shorter overall survival (Cox proportional hazards, $P = 7.3 \times 10^{-6}$), as previously shown (14, 15).

Finally, an analysis for genomically integrated viral sequences, including SV40, was negative (Supplementary Section 8), as was a screen of exome and RNA-sequencing data for evidence of *EWSR1* and *ALK* fusions, recently reported in rare cases of MPM (16, 17) and peritoneal mesothelioma (18), respectively. As well, no activating mutations in the canonical MAPK or PI3K/AKT signaling pathways were identified in this cohort.

Comprehensive Analysis of *BAP1* Status in MPM

BAP1, encoding a nuclear deubiquitinase, is the most frequently mutated cancer gene in MPM, in both our data set and others (5), and is also recurrently inactivated in clear cell renal carcinoma, uveal melanoma, and cholangiocarcinoma (19). Somatic *BAP1* mutations have germline counterparts that define the *BAP1* hereditary cancer syndrome (20). In contrast to other cancers, *BAP1* inactivation in MPM does not correlate with adverse outcomes. Because its role in MPM biology remains unclear, we compared *BAP1*-inactivated and wild-type cases across multiple platforms. First, to better segregate cases according to *BAP1* status, we performed a comprehensive analysis of inactivating alterations through a detailed review of single-nucleotide variants, small and large indels, whole gene deletions, and structural variants; this showed the overall prevalence of *BAP1* alterations to be 57% (Fig. 1A; Supplementary Table S2A), in line with recent studies (21). Most MPM with inactivating mutations in *BAP1* (25/26, 96%) also had concurrent loss of heterozygosity (LOH) on chromosome 3p21.1, supporting a classic two-hit tumor suppressor mechanism. Overall, *BAP1* status was defined as follows: 32 samples with no evidence of *BAP1* alteration, 6 with a single (heterozygous) mutation or deletion, and 36 with biallelic inactivation. No germline mutations in *BAP1* were identified in this cohort.

BAP1 alterations showed nonrandom patterns of co-occurrence with mutations in other key MPM cancer genes (Fig. 2A). As expected, mRNA expression levels of *BAP1* itself were reduced in the presence of genomic *BAP1* inactivation or loss (Fig. 2B). We also observed an inverse correlation of *BAP1* alterations and SCNAs. *BAP1*-altered tumors had fewer chromosome arm gains and losses (Fig. 2C, median 9.5 vs. 15.5, Mann–Whitney, $P < 0.01$), as well as fewer focal SCNAs (Supplementary Fig. S2).

Because BAP1-mediated deubiquitination of histones and transcriptional proteins is thought to regulate gene expression, we compared mRNA expression patterns between tumors that were wild-type for *BAP1* and those with inactivation of one or both *BAP1* alleles. We identified 1,324 differentially expressed genes with an FDR of <0.01, of which 75% were downregulated in the *BAP1*-inactivated samples. As previously noted in experimental models (22), *BAP1*-inactivated tumors in our cohort had lower mRNA expression of several HOXA genes, including *HOXA5* and *HOXA6*, but no difference in *EZH2* mRNA expression or its PRC2 partners *EED* and *SUZ12*.

As BAP1 is known to regulate the ubiquitination and hence stability of several transcriptional proteins, we examined the association of *BAP1* status with inferred activity of transcription factors (TF) using a recently developed computational strategy that integrates phosphoproteomic and transcriptomic data with predicted TF binding sites (23). We used this algorithm to assess significant differences in inferred TF activities between *BAP1*-inactivated and wild-type MPM (satisfying FDR-corrected $P < 0.01$, t test), linking *BAP1* status to altered activity of TFs. Indeed, many TFs identified in this analysis had highly significant associations with *BAP1* status (Fig. 2D and E; Supplementary Table S2B).

In particular, YY1 had significantly reduced inferred activity in *BAP1*-inactivated samples (Fig. 2F). BAP1 forms a

Downloaded from http://aacrjournals.org/cancerdiscovery/article-pdf/8/12/1548/1728852/1548.pdf by guest on 20 August 2022

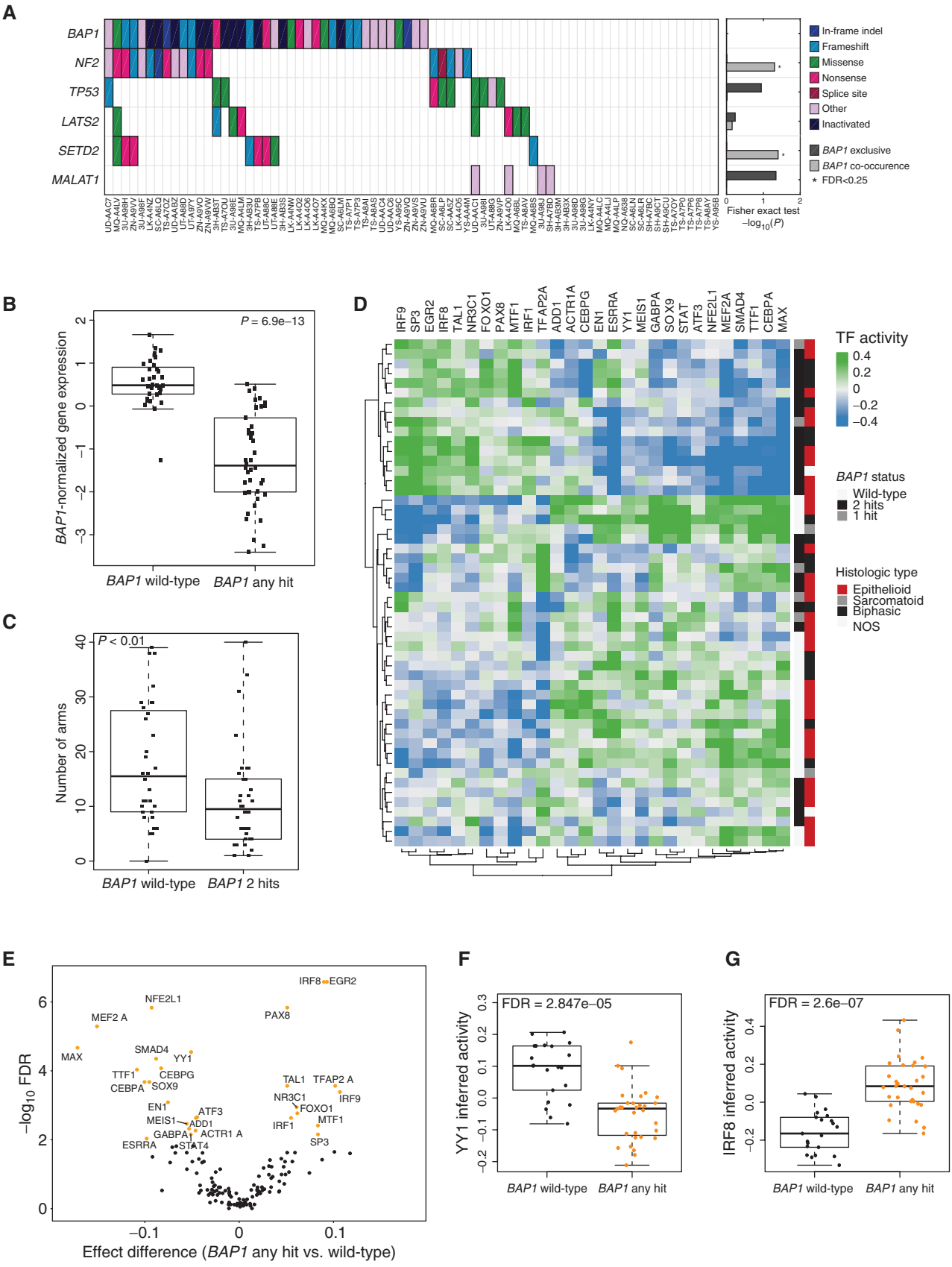

Downloaded from http://aacrjournals.org/cancerdiscovery/article-pdf/8/12/1548/1728852/1548.pdf by guest on 20 August 2022

ternary complex with HCF1 and YY1, which acts as transcriptional repressor of genes involved in cell proliferation (24). YY1 has also been shown to regulate or interact with other TFs whose inferred activity was also altered in our analysis, such as MAX and EGR2. Moreover, there is evidence that YY1 interacts with EZH2, the catalytic subunit of PRC2, and is required for its function in gene silencing (25). Thus, to a degree, the transcriptional consequences of *BAP1* inactivation could be attributed to changes in recruitment of specific TFs to their target genes, either directly, as in the loss of ternary YY1–HCF1–BAP1 complexes, or indirectly, as in the case of TFs that are themselves downstream targets of YY1 (Supplementary Table S2C).

Notably, *BAP1*-inactivated samples demonstrated a significantly increased inferred activity of IRF8 (Fig. 2G; Supplementary Table S2D), a hematopoietic lineage TF involved in interferon signaling and dendritic cell differentiation. Both pathways were upregulated in our *BAP1*-based supervised gene mRNA expression analysis (see above). Moreover, PARADIGM analysis confirmed that the IRF activation pathways are upregulated in *BAP1*-inactivated samples. IRF8 has been implicated in the biology of CD103-positive dendritic cells whose antigen-presenting function is highly effective at stimulating cytotoxic T cells in the tumor microenvironment (26). Taken together, these observations suggest an association between *BAP1* status and perturbed immune signaling in MPM that warrants further exploration.

MPM with Genomic Near-Haploidization, a Novel Subtype

Allele-specific copy-number analysis of WES data using the FACETS algorithm (27) identified three cases with striking genome-wide LOH that affected more than 80% of the genome, which was confirmed in SNP6.0 copy-number array data (Fig. 3A and B; Supplementary Fig. S2). This phenomenon, well described in acute lymphoblastic leukemia (28), occurs when the nascent cancer clone loses one copy of nearly all chromosomes [which we term "genomic near-haploidization" (GNH)] followed by duplication of the remaining chromosomes. To better assess the prevalence of this unusual genomic phenomenon in MPM, we screened 80 samples from a Japanese International Cancer Genome Consortium (ICGC) MPM cohort, identifying two additional cases (Fig. 3B), representing a combined prevalence of 5 of 154 (3.2%). Neither the three TCGA cases, nor the two ICGC cases, had deletions or point mutations in *BAP1, PBRM1,* or *SETD2*. Remarkably, all 5 cases had inactivating point mutations in, or homozygous deletion of, *SETDB1*, which encodes a histone methyltransferase involved in gene silencing, representing the only *SETDB1*-mutated MPMs in the combined TCGA–ICGC cohort. Additionally, 4 of 5 cases with evidence of GNH had driver mutations in *TP53*. Although near-haploid cases have been reported in other cancers (e.g., acute lymphoblastic leukemia, chondrosarcoma, and adrenocortical carcinoma), the strong association of *TP53* and *SETDB1* comutation with widespread LOH has not been previously reported in other cancers (28, 29).

To further define the clinical features of this novel subset, we obtained data on 16 additional cases with near-haploid karyotypes from a large independent series of MPM studied by cytogenetic analysis of short-term primary cultures (Supplementary Section 2.2; note: cytogenetic analysis can identify only GNH cases that have not undergone genome duplication). Although most of the genome in our 5 cases showed LOH, chromosomes 5 and 7 strikingly retained heterozygosity (Fig. 3C). These two chromosomes also remained disomic in the cases with near-haploid karyotypes in the independent cytogenetic series (Supplementary Table S3). Based on this combined set of 21 near-haploid MPM, a distinctive profile of genomic and clinical features emerged, demarcating a novel molecular subtype of MPM. Strikingly, most patients with MPM showing GNH were female (M:F = 1:4), in sharp contrast to the overall TCGA–ICGC MPM cohort, where males greatly predominated (M:F > 4:1; $P < 0.01$, Fisher exact test). No difference in distribution of histologic types was observed in the GNH subset.

Because MPM with evidence of GNH have typically undergone a genome-doubling event, we were able to assess the timing of this relative to point mutations (30, 31). Essentially, mutations acquired before genome duplication would be present on both copies of the duplicated chromosome, whereas those occurring after would be heterozygous. In all three TCGA cases with GNH, the majority of the point mutations were present on both copies of duplicated chromosomes, suggesting that the genome duplication occurred relatively late in the evolution of the cancer. In three cases, the *TP53* driver mutation was homozygous, suggesting it occurred before genome doubling. In contrast, the *SETDB1* mutations were present on only one of the two copies of chromosome 1 in two of the three cases, suggesting they occurred after LOH

Downloaded from http://aacrjournals.org/cancerdiscovery/article-pdf/8/12/1548/1728852/1548.pdf by guest on 20 August 2022

Figure 2. Supervised comparisons between *BAP1*-inactivated and wild-type MPM. **A,** *BAP1* inactivation by copy-number loss or mutation across the cohort, along with mutations in 6 other genes (left). These genes were selected as those with more than 3 nonsilent mutated tumors. Large genes with more than 3 kb coding regions (*TTN*, *FAT4*, and *MGA*) are unlikely to be functional in cancer and were excluded. The bar plot (right) shows the Fisher exact test *P* values for mutual exclusivity and co-occurrence relative to *BAP1*. Only *SETD2* and *NF2* approach significant co-occurrence with *BAP1* inactivation. The one-tail Fisher *P* values for co-occurrence and the Benjamini–Hochberg FDRs are $P = 0.04$, FDR = 0.15 for *SETD2* and $P = 0.05$, FDR = 0.15 for *NF2*. We detected *MALAT1* (aka *NEAT2*) "RNA" mutations in 4 *BAP1*-inactivated samples, but this does not reach significance ($P = 0.05$, FDR ~0.27). **B,** Normalized *BAP1* mRNA expression levels in the wild-type, 1 hit and 2 hit subgroups. **C,** Box plot demonstrating a significantly lower frequency of arm-level losses in *BAP1*-inactivated tumors (BAP1 2 hits) compared with wild-type (BAP1 0). **D,** Inferred transcription factor (TF) activities significantly associated with *BAP1* inactivation (FDR < 0.01). **E,** Volcano plot with mean inferred TF activity difference in *BAP1*-inactivated and *BAP1* wild-type patients plotted on the *x*-axis, and FDR-adjusted significance from *t* test plotted on the *y*-axis ($-\log_{10}$ scale). TFs significantly associated with *BAP1* inactivation status (FDR < 0.01) are colored in orange. **F** and **G,** Box plots with differential inferred activities of YY1 (**F**) and IRF8 (**G**), two biologically relevant transcription factors. The target genes on which inferences for YY1 (427 genes) and IRF8 (248 genes) activity were based are provided in Supplementary Table S2.

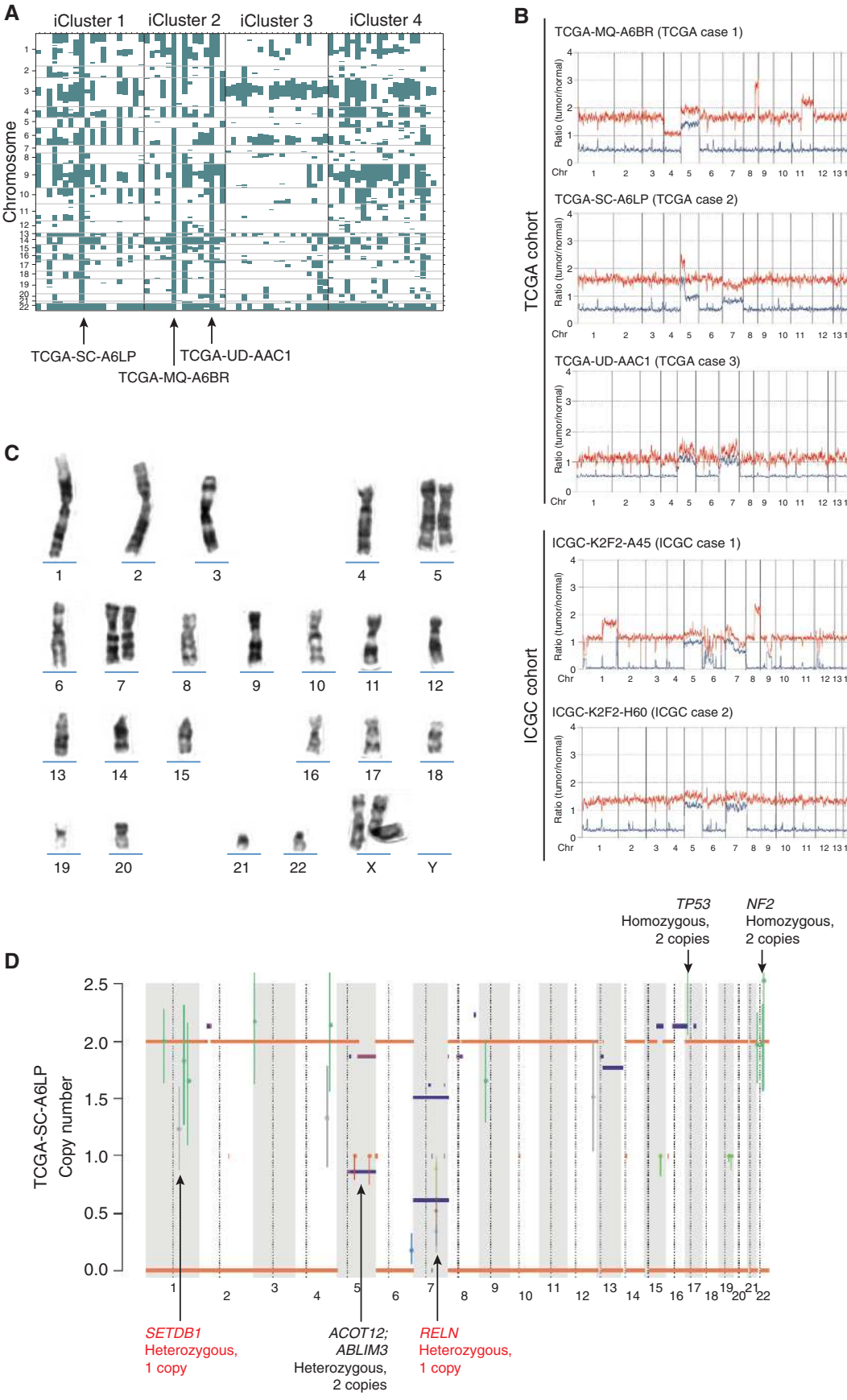

Downloaded from http://aacrjournals.org/cancerdiscovery/article-pdf/8/12/1548/1728852/1548.pdf by guest on 20 August 2022

and genome duplication (Fig. 3D). Overall, these data suggest a model in which *TP53* mutations occur early, and presumably permit the steady (or catastrophic) loss of chromosomes. It seems likely that genome reduplication occurs after achieving near-haploidy, with haploinsufficiency of *SETDB1* arising later.

Integrative Multiplatform Analysis Defines Novel Prognostic Subsets

Although the current classification of MPM into epithelioid, sarcomatoid, and biphasic histologies is prognostically useful, there remains variability in clinical features and patient outcomes within histologic subtypes. Previous analyses (5, 7) based on mRNA expression alone have defined unsupervised clusters largely recapitulating these histologic distinctions. To find out whether multiplatform molecular profiling might provide additional resolution to define prognostic subsets of MPM, we performed integrative clustering across multiple assay platforms using two algorithms: iCluster (32) and PARADIGM (33). Both identified four distinct integrated subtypes of MPM. There was a strong concordance in subtype assignments between the two algorithms (Fig. 4A; Supplementary Figs. S6 and S7), especially for the best (cluster 1) and worst (cluster 4) prognosis clusters, indicating that integration of molecular data can identify distinct subgroups of MPM, independent of the specific statistical methodology. Survival was significantly different across the 4 clusters ($P < 0.0001$ for either algorithm; Fig. 4B; Supplementary Fig. S7). This survival difference remained significant ($P = 0.008$) after adjusting for histology (epithelioid vs. nonepithelioid) and *CDKN2A* homozygous deletion (Fig. 4C; Supplementary Fig. S6), a known molecular prognostic factor in MPM (14, 15). Although they did provide additional independent prognostic information, the iClusters nonetheless did show correlation with consensus histology ($P = 0.002$), with iCluster cluster 1 being enriched for epithelioid histology (similar finding for PARADIGM cluster 1). They also exhibited differences in immune cell infiltrates (Supplementary Table S4A), as discussed below, but showed no significant correlation with clinical variables such as T stage, N stage, asbestos exposure history, or smoking (Supplementary Table S4B). Molecularly, these tumors had low SCNA, relatively few *CDKN2A* homozygous deletions (11%), and a high level of methylation (Supplementary Fig. S4). All but one (95%) had *BAP1* alterations: 26% had homozygous deletions and 53% had heterozygous loss with mutations.

The poor prognosis cluster (cluster 4; red) had a high score for epithelial–mesenchymal transition (EMT) based on gene expression ($P < 0.001$; Fig. 4D), which was distinguished by high mRNA expression of *VIM, PECAM1,* and *TGFB1*, and low miR-200 family expression. These tumors also displayed *MSLN* promoter methylation and consequent low mRNA expression of mesothelin, a marker of differentiated mesothelial cells, as noted previously in sarcomatoid MPM and the sarcomatoid components of biphasic MPM (15, 34). Overall, this poor prognosis cluster also showed enrichment of *LATS2* mutations (30% compared with 4% in the rest of the cohort) and *CDKN2A* homozygous deletions (66%). Moreover, this cluster showed higher *AURKA* mRNA expression, higher leukocyte fraction (based on DNA methylation), and elevated mRNA expression of E2F targets, G_2–M checkpoints, and DNA damage response genes. PI3K–mTOR and RAS–MAPK signaling were upregulated, based on both mRNA and protein expression (Supplementary Fig. S7). Additionally, several miRNAs were differentially expressed between the good and poor prognostic clusters, including miR-193a-3p, which has been proposed as a potential tumor suppressor (35). Finally, a comparison of immune gene mRNA expression signatures (36) across the four clusters revealed a significantly higher score for the Th2 cell signature in the poor prognosis cluster 4 compared with the other clusters (Fig. 4E; Supplementary Table S4A). Coincidentally, it has been reported that Th2 cytokines secreted by immune cells upon exposure to asbestos may promote MPM (37). The analyses of other immune signatures are shown in Supplementary Fig. S5.

Although biphasic and sarcomatoid MPM are more aggressive, there remains a need for improved risk stratification of epithelioid MPM, for which clinical outcomes are more heterogeneous. Therefore, we conducted an integrative clustering analysis restricted to epithelioid MPM. The results for the 4-cluster epithelioid-only solution were highly similar to the 4-cluster all-MPM solution (Fig. 5A), with only 7 of the 52 epithelioid samples reassigned to other clusters. This stability indicates that the features driving the all-MPM clustering are largely independent of histology. The epithelioid-only clusters share many of the features defining the corresponding clusters in the all-MPM solution (Fig. 5B). The survival analysis also paralleled the all-MPM solution, with cluster 1 having the best outcomes and cluster 4 having the worst (Fig. 5C). PARADIGM analysis of the epithelioid-only subset confirmed upregulation of *AURKA* mRNA expression in the poor-prognosis epithelioid-only cluster 4 (Fig. 5D), corroborating the results from the all-MPM analysis.

Finally, we sought to independently validate the clinical correlations of clusters identified in the TCGA epithelioid cases using mRNA expression profiles from two published studies: 211 MPM analyzed by RNA sequencing (5) and 52 MPM samples analyzed by mRNA expression microarrays (14). Specifically, we assigned each mRNA expression profile to one of the integrative clusters based on the rules derived from the TCGA mRNA data set. For the larger validation cohort (henceforth referred to as Bueno), we restricted our analysis to epithelioid samples and used the epithelioid-only gene signature to cluster samples. We found that the epithelioid-only samples assigned

Figure 3. MPM cases with GNH. **A,** WES-based LOH profiling with the FACETS algorithm revealed three MPM samples with genome-wide LOH. **B,** Allelic copy-number plots of genome-wide LOH cases in the TCGA and Japanese ICGC cohorts. X-axis and y-axis are the chromosome locations, and the ratio of an allelic copy number of tumor sample to that of matched normal control (lymphocyte), respectively. Red line shows the higher allele, and blue line shows the lower allele. **C,** Near-haploid metaphase cell derived from the Brigham and Women's Hospital genome-wide LOH cohort, stained by Giemsa, showing loss of one copy of all chromosomes except 5, 7, and X. **D,** Allelic copy-number plot of a representative TCGA case with biallelic inactivation of *TP53* and monoallelic mutation of *SETDB1*, suggesting the latter occurred after the LOH and genome duplication events.

Downloaded from http://aacrjournals.org/cancerdiscovery/article-pdf/8/12/1548/1728852/1548.pdf by guest on 20 August 2022

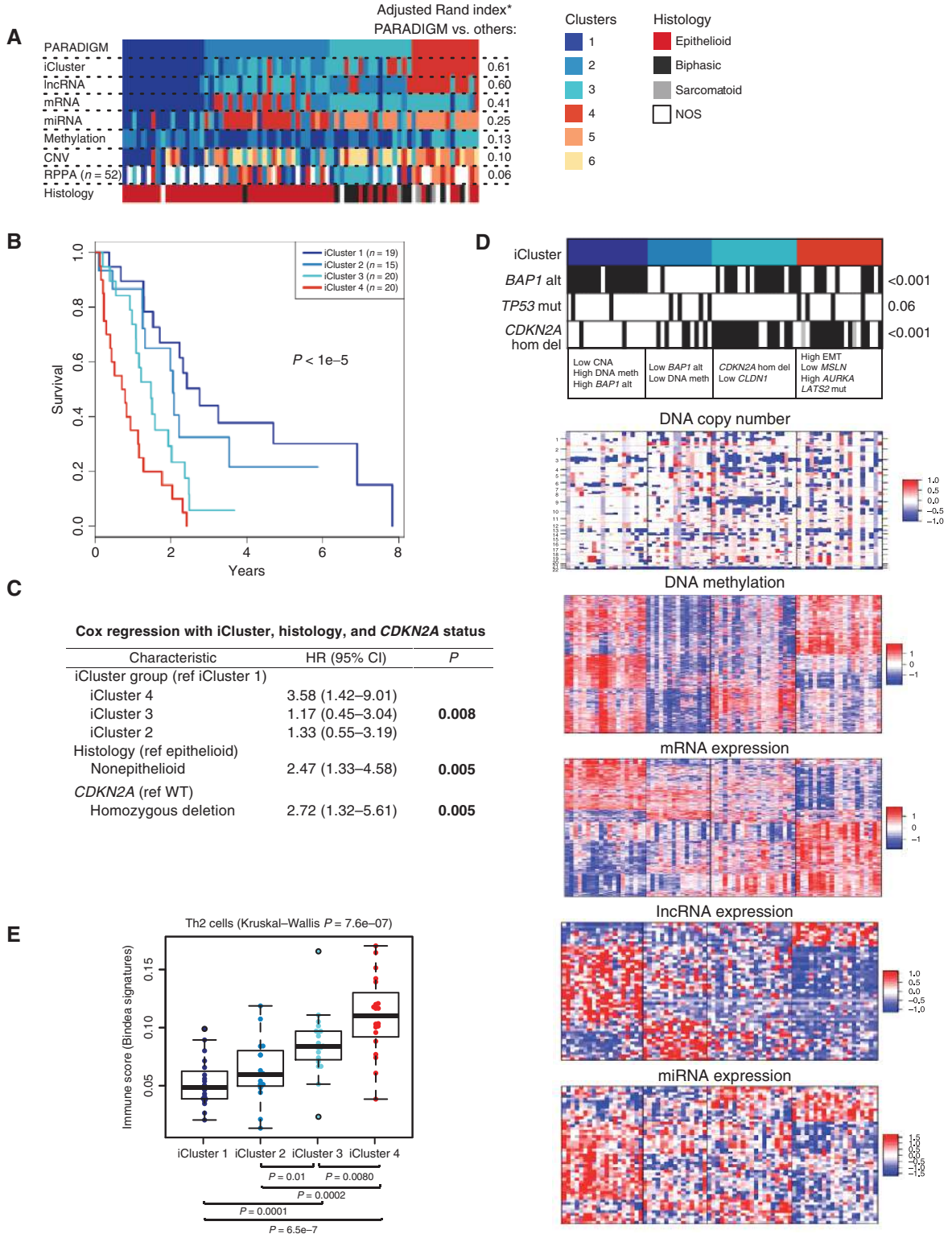

Figure 4. Integrative analysis of 74 MPM. **A,** Concordance between integrative (PARADIGM and iCluster) and platform-specific unsupervised clustering results. Clusters are color-coded and ranked based on survival (dark blue indicates best survival, and red and orange mark the worst surviving subgroup). CNV, copy-number variation. **B,** Kaplan–Meier plot of the integrative subgroups reveals distinct outcomes. **C,** Cox regression analysis demonstrates significant associations of the molecular subtypes with patient survival, even upon adjusting for histology, age, and *CDKN2A* status. **D,** iCluster identified 4 integrative subgroups with distinct *BAP1* alteration (defined as mutation and/or copy-number alteration), *TP53* mutation, *CDKN2A* status, copy-number alteration, DNA methylation, and mRNA, lncRNA, and miRNA expression profiles. **E,** Comparison of Th2 cell immune gene mRNA expression signature across the four integrated clusters.

Downloaded from http://aacrjournals.org/cancerdiscovery/article-pdf/8/12/1548/1728852/1548.pdf by guest on 20 August 2022

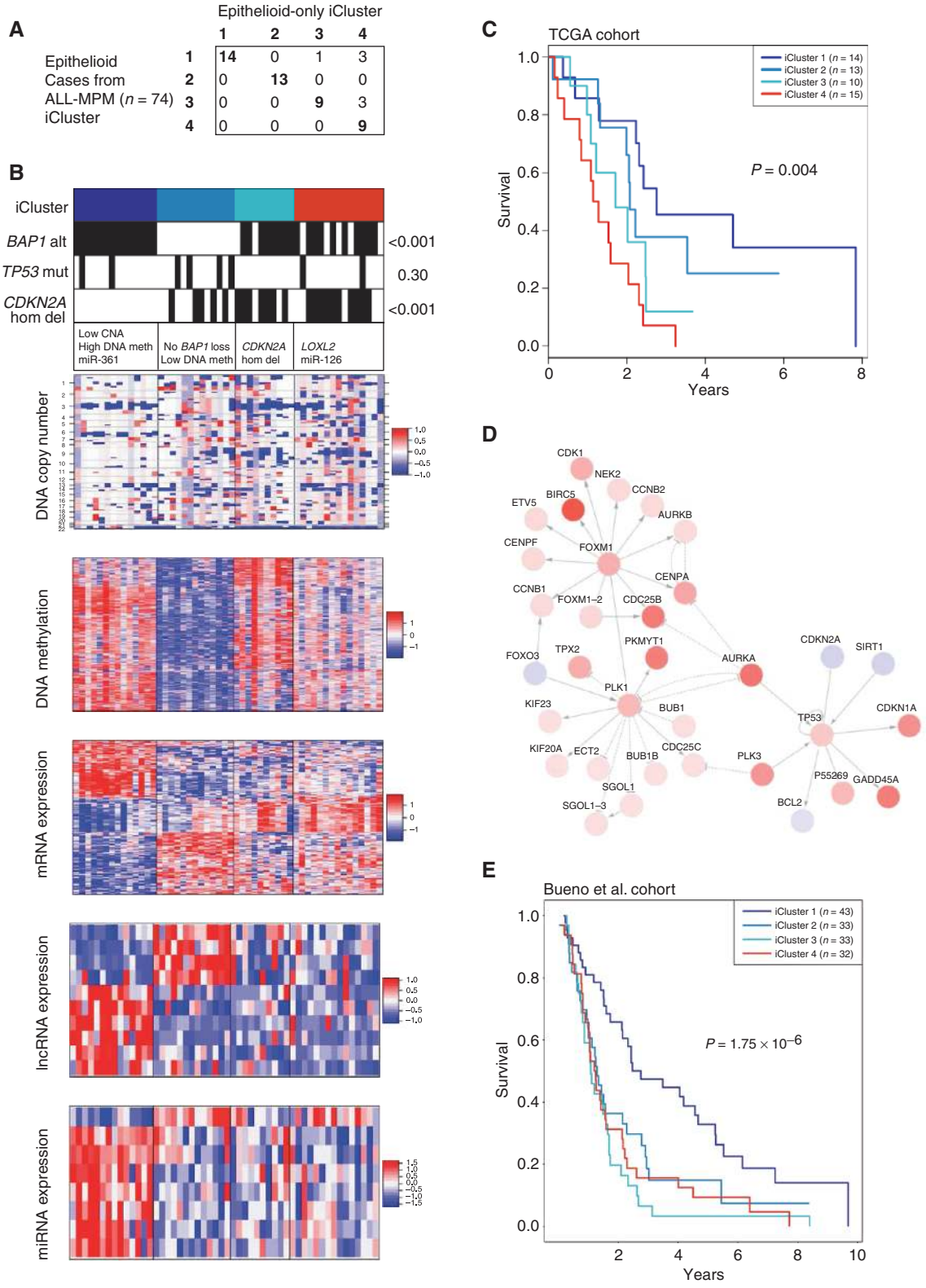

Figure 5. Integrative analysis of epithelioid MPM. **A,** Comparison of cluster assignments between the epithelioid-only and full cohort integrative analyses demonstrating good concordance, with only 7 cases being reassigned to another cluster. **B,** Integrative clustering analysis applied to cases with epithelioid histology. **C,** Kaplan–Meier plot of the epithelioid-only integrative subgroups. **D,** PATHMARK analysis revealed differentially active molecular pathways that define the poor-prognosis epithelioid-only subgroup. **E,** Validation of the TCGA epithelioid subtypes in an independent cohort of 141 epithelioid MPM (Bueno et al.; ref. 5) confirming the protective effect of molecular features that define iCluster 1.

Downloaded from http://aacrjournals.org/cancerdiscovery/article-pdf/8/12/1548/1728852/1548.pdf by guest on 20 August 2022

to iCluster 1 (good prognosis) had significantly better survival, even after adjusting for age ($P = 3.9 \times 10^{-4}$; Fig. 5E; Supplementary Fig. S6). In the smaller cohort (referred to as Lopez-Rios), patient numbers were too small to split by histology. However, this analysis provided independent validation of the survival differences for the four all-MPM clusters ($P = 0.01$; Supplementary Fig. S6). Taken together, these results suggest that the prognostically relevant molecular profiles defined by our analysis are robust and reproducible, and could potentially be used to improve risk stratification of patients with epithelioid MPM. The core mRNA gene lists are provided in Supplementary Table S4C–S4G, which also include reduced classifiers based on methylation, lncRNA, miRNA, and a reduced classifier combining mRNA and methylation data to facilitate practical application of these data and independent validation of these clusters.

Analysis of Noncoding RNAs in MPM

We next assessed two types of noncoding RNAs not extensively studied in MPM that may also represent a source of robust biomarkers: lncRNAs, which often show higher expression specificity for cell type than coding genes, and miRNAs, which are relatively stable in biological fluids, so potentially suitable as noninvasive biomarkers.

In both the TCGA and Bueno (5) cohorts, lncRNAs returned four unsupervised consensus subtypes that were associated with 5-year survival ($P = 1.4 \times 10^{-10}$ and $P = 1.1 \times 10^{-3}$, respectively). The TCGA lncRNA subtypes were highly concordant with iCluster ($P = 8 \times 10^{-14}$) and PARADIGM ($P = 2 \times 10^{-21}$) subtypes and were associated with EMT scores ($P = 2.5 \times 10^{-6}$; Figs. 4A, 6A–E; Supplementary Table S5A.1). For both cohorts, lncRNAs that were differentially abundant between the good-prognosis subtype and other samples included those associated with cancer (e.g., *H19*, *LINC00152*, and *MEG3*), or with MPM in particular: *NEAT1* and *SNHG8* (38) and *GAS5* (ref. 39; Fig. 6F and G; Supplementary Table S5B.3-6). We noted that a number of lncRNAs distinguished the good-prognosis cluster in both TCGA and Bueno cohorts (Supplementary Table S5B.1-2,5-6).

Unsupervised clustering based on miRNA mature strands resolved five consensus subtypes in the TCGA cohort (Fig. 6H); these were associated with 5-year survival ($P = 7 \times 10^{-4}$), iCluster ($P = 1 \times 10^{-12}$) and PARADIGM ($P = 3 \times 10^{-13}$) clusters, and EMT scores ($P = 2 \times 10^{-7}$; Fig. 6H–K; Supplementary Table S5A.2). For the good-survival cases, the miRNA subtypes were strikingly concordant across multiple analysis platforms, and many cancer-associated miRNAs were differentially abundant in the good-survival cluster (Fig. 6L; Supplementary Table S5B.3-4). Taken together, these results suggest that lncRNAs and miRNAs may be important predictors of survival in MPM.

EMT and VISTA Expression

Because mRNA expression of EMT-associated genes was a key differentiating feature between prognostically distinct integrative clusters, we performed a detailed analysis of EMT in MPM using a previously published EMT-related mRNA signature (40). Increasing EMT scores significantly correlated with clusters defined by integrative algorithms (iCluster and PARADIGM), as well as with individual genomic features including miRNA, lncRNA, methylation, RPPA, and overall gene expression (Fig. 7A). Of all tumor types included in the TCGA pan-cancer analysis, MPM had the second-highest average EMT score (Fig. 7B; after soft-tissue sarcomas), consistent with previous reports that EMT is a frequent phenomenon in MPM (7, 41).

Although EMT score positively correlated with the mRNA expression of many immune-regulatory genes, such as *OX40L, TGFB1, CD276, OX40,* and *PD-L2* ($P < 0.001$; Fig. 7A and C), mRNA expression of *VISTA* (42), a negative immune-checkpoint regulator primarily expressed on hematopoietic cells (43), was strongly inversely correlated with EMT score (Fig. 7C) and was expressed at levels higher than in any other TCGA tumor type analyzed (Fig. 7D). In the MPM cohort, *VISTA* mRNA levels were highest in the epithelioid subtype (Fig. 7C and E). Using Regulome Explorer (Supplementary Section 13), we found that *VISTA* mRNA expression was highly correlated with *MSLN* mRNA expression (Spearman correlation = 0.81; $P = 6.3 \times 10^{-19}$), but not with mRNA expression of PD-1 or PD-L1. Moreover, there was no significant correlation between overall mutation burden and *VISTA* expression levels ($P = 0.64$).

VISTA (V-domain Ig suppressor of T-cell activation; also known as c10orf54, PD-1H, and B7-H5) is a member of the B7 family of negative checkpoint regulators, expressed on the surface of several immune cell types. It can function as both receptor and ligand (44). As a ligand, VISTA is present on the surface of antigen-presenting cells (APC) and inhibits early-stage T-cell activation (45). The normal mesothelium has APC properties (46), which are retained upon malignant transformation (47, 48). We thus performed IHC staining of two epithelioid TCGA MPM cases, as well as normal and reactive mesothelium (Supplementary Section 14), to define the cellular compartment expressing VISTA in MPM tumor samples. Remarkably, VISTA protein expression was not restricted to infiltrating immune cells, but was present in tumor cells in MPM, as well as in normal and reactive mesothelium (Fig. 7F and G), suggesting that its expression in epithelioid MPM may reflect retention of APC properties in this more differentiated subset of MPM.

DISCUSSION

Our comprehensive integrative analysis of 74 cases of MPM further defines a cancer driven primarily by inactivation of tumor suppressor genes. Indeed, we confirm the high frequency of *BAP1* inactivation by mutation and copy-number loss, as well as recurrent inactivating alterations in *CDKN2A, NF2, TP53, LATS2,* and *SETD2.* In addition to this landscape of known loss-of-function events, we have genomically characterized a novel molecular subtype of MPM accounting for approximately 3% of MPM in our data sets, defined by evidence of genomic near-haploidization and recurrent *TP53* and *SETDB1* mutations, with a distinctive clinical phenotype showing female predominance and younger age at diagnosis. Our findings should facilitate systematic clinical studies of this subset to better define its survival and its association with asbestos exposure, which so far appears weak or unclear. Isolated cases with similar molecular profiles (GNH and *SETDB1* mutation) have been anecdotally reported (5, 49),

Downloaded from http://aacrjournals.org/cancerdiscovery/article-pdf/8/12/1548/1728852/1548.pdf by guest on 20 August 2022

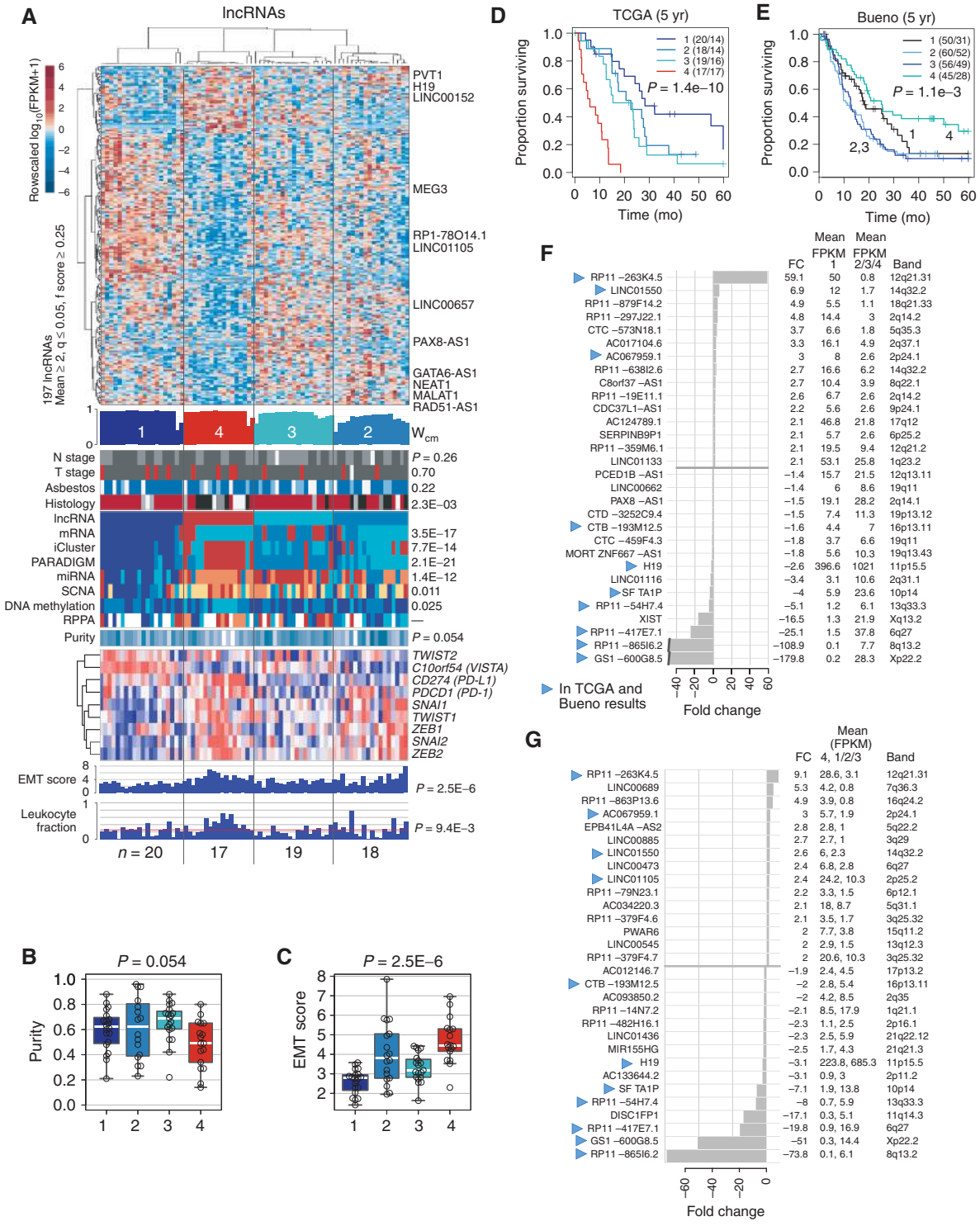

Figure 6. Noncoding RNA subtypes and differential abundance for lncRNAs and miRNAs in the TCGA and Bueno cohorts. **A–G,** lncRNA subtypes and differential abundance. **A,** Top to bottom: Normalized abundance heat map for a 4-subtype solution, then a silhouette width profile (Wcm) calculated from the consensus membership matrix; clinical and molecular covariates, with *P* values from Fisher exact, χ^2, or Kruskal tests; and profiles of RNA-sequencing–based EMT scores and leukocyte fraction. Red horizontal line in leukocyte fraction bar plot indicates the median value across all samples. **B,** Distribution of purity estimated by ABSOLUTE, with a Kruskal *P* value. **C,** Distribution of RNA-sequencing–based EMT scores, with a Kruskal *P* value. **D,** Kaplan–Meier plot for overall survival, with a log-rank *P* value. **E,** Kaplan–Meier plot for overall survival, with a log-rank *P* value for a 4-subtype solution for the Bueno cohort. **F** and **G,** lncRNAs that were differentially abundant (SAM 2-class unpaired analysis, FDR < 0.05) between the better-survival lncRNA subtype and all other samples, for the TCGA cohort (**F**) and the Bueno cohort (**G**). The largest 15 positive and 15 negative fold changes are shown; blue triangles mark lncRNAs that were in these gene sets in results for both cohorts. Text to the right of each bar plot gives means-based fold changes, mean abundance in the target and then the other samples, and the cytoband for the gene. See also Supplementary Table S5A. (*continued on next page*)

Downloaded from http://aacrjournals.org/cancerdiscovery/article-pdf/8/12/1548/1728852/1548.pdf by guest on 20 August 2022

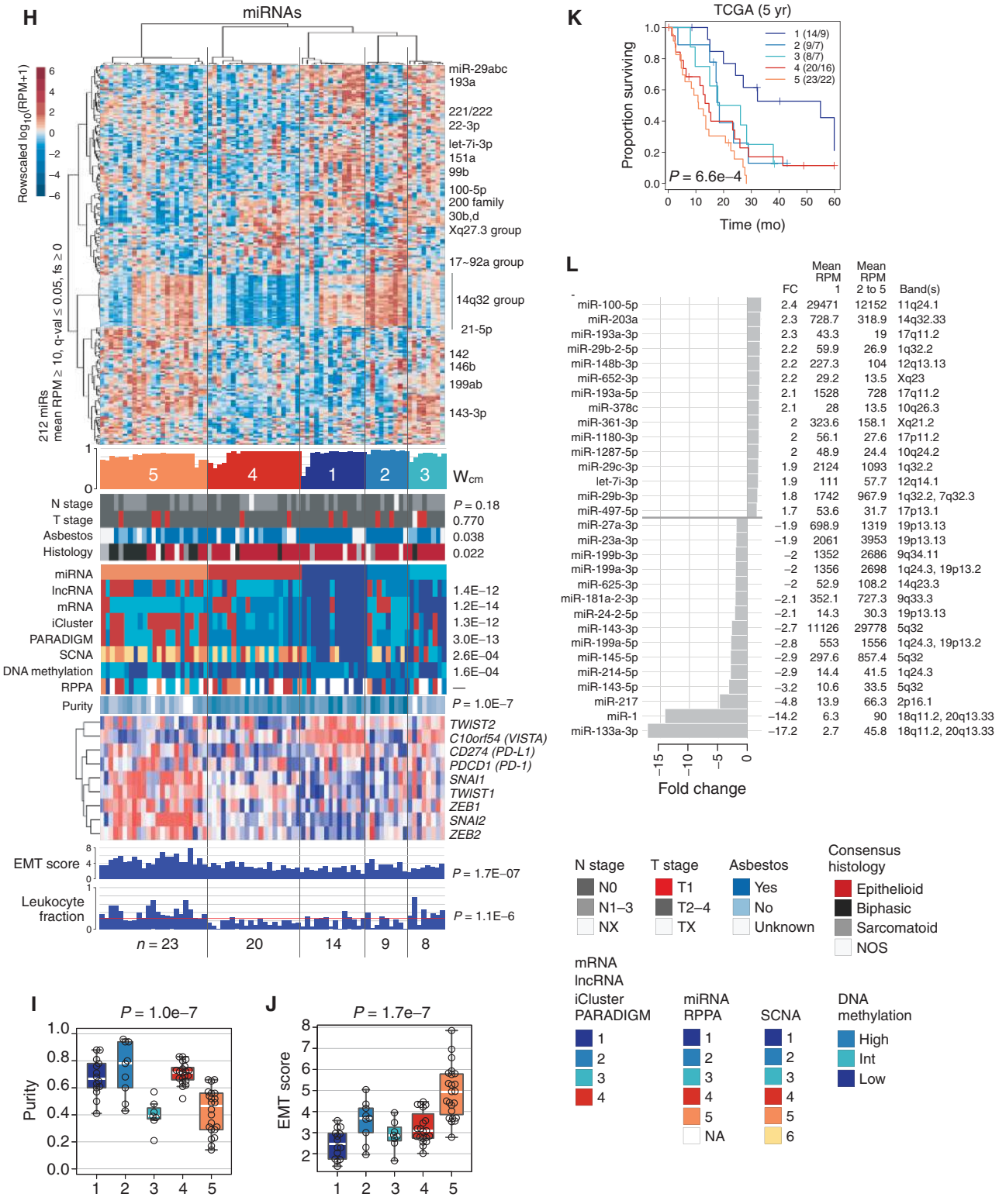

Figure 6. ***(Continued)*** **H–L,** microRNA mature strand subtypes and differential abundance in the TCGA cohort. **H,** Top to bottom: Normalized abundance heat map for a 5-subtype solution, then a silhouette width profile (Wcm) calculated from the consensus membership matrix; clinical and molecular covariates, with *P* values from Fisher exact, χ^2, or Kruskal tests; and profiles of RNA-sequencing–based EMT scores and leukocyte fraction. Red horizontal line in leukocyte fraction bar plot indicates the median value across all samples. **I,** Distribution of purity estimated by ABSOLUTE, with a Kruskal *P* value. **J,** Distribution of RNA-sequencing–based EMT scores, with a Kruskal *P* value. **K,** Kaplan–Meier plot for overall survival, with a log-rank *P* value. **L,** miRNA mature strands that were differentially abundant between the better-survival lncRNA subtype and all other samples, for the TCGA cohort. The largest 15 positive and 15 negative fold changes are shown. Text to the right of each bar plot gives means-based fold changes, mean abundance in the target and then the other samples, and the cytoband(s) for the mature strand. See also Supplementary Table S5B.

Downloaded from http://aacrjournals.org/cancerdiscovery/article-pdf/8/12/1548/1728852/1548.pdf by guest on 20 August 2022

but had not, until now, been recognized as a distinct molecular subtype of MPM. The genomic data in our cases support a model in which early *TP53* mutations are permissive for a loss of chromosomes to a near-haploid state, followed by genome reduplication and *SETDB1* inactivation. As H3K9 methylation by SETDB1 is a repressive chromatin mark (50), it is tempting to speculate that inactivation of SETDB1 allows a general increase in transcription activity in a cancer cell that has sacrificed nearly half of its genome, presumably including several genes that are imprinted or otherwise monoallelically

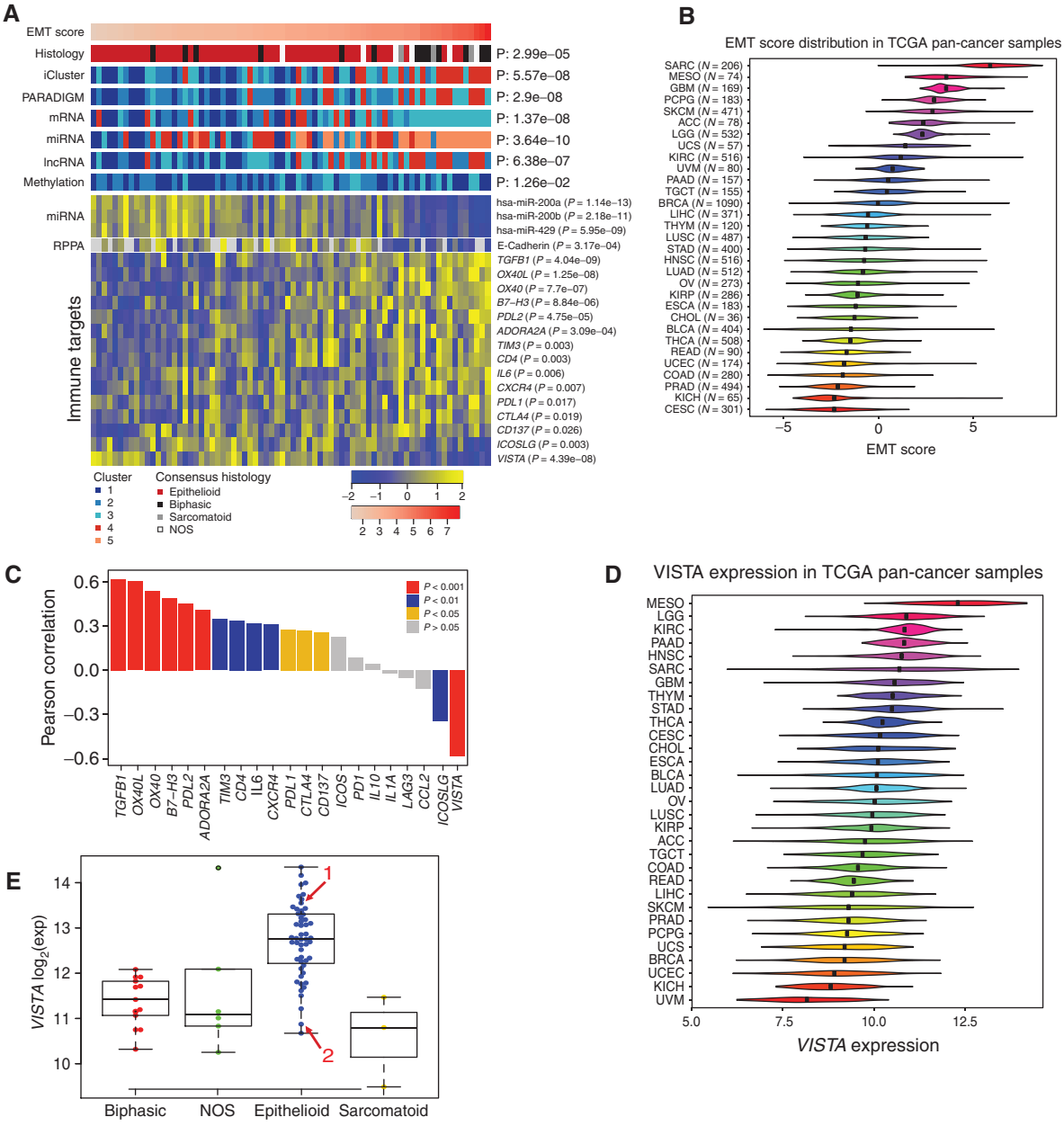

Figure 7. MPM is enriched for both EMT and mRNA expression of immune targets. **A,** Unsupervised analysis identifies correlations between EMT and multiple platforms. Tumors are ordered from left to right according to increasing EMT score. Numbered color bars indicate group assignments (clusters) from other data types. Statistically significant correlations are shown between EMT score and (starting at top) integrative multidimensional analyses on both iCluster and PARADIGM platforms, along with mRNA, miRNA and lncRNA clusters, methylation status, and consensus histology. Bottom plots illustrate significant correlations between these clusters and selected miRNAs, proteins, immune target genes. **B,** Spectra of EMT scores across different tumor types. Mesothelioma is the second most mesenchymal cancer type after sarcoma in 31 tumor types analyzed. Despite most MPM tumors having undergone EMT, a broad range of EMT scores were observed across mesothelioma cases, which corresponded to a large extent with histologic subtype. **C,** Waterfall plot illustrating the correlation between EMT and immune target genes. **D,** Plot highlighting *VISTA* mRNA expression, which is highest in MPM, across all TCGA tumor types. **E,** Box plot indicating *VISTA* mRNA expression levels in individual histologic types of the TCGA MPM cohort. The highest mRNA expression levels were observed in the epithelioid subtype (Wilcoxon rank-sum, $P = 2e{-}7$), whereas sarcomatoid MPM had the lowest mRNA expression ($P = 0.017$). Red arrows indicate two epithelioid cases that were examined by immunohistochemistry, TCGA-SC-A6LQ-01 (1) and TCGA-SC-A6LM-01 (2). (*continued on next page*)

Downloaded from http://aacrjournals.org/cancerdiscovery/article-pdf/8/12/1548/1728852/1548.pdf by guest on 20 August 2022

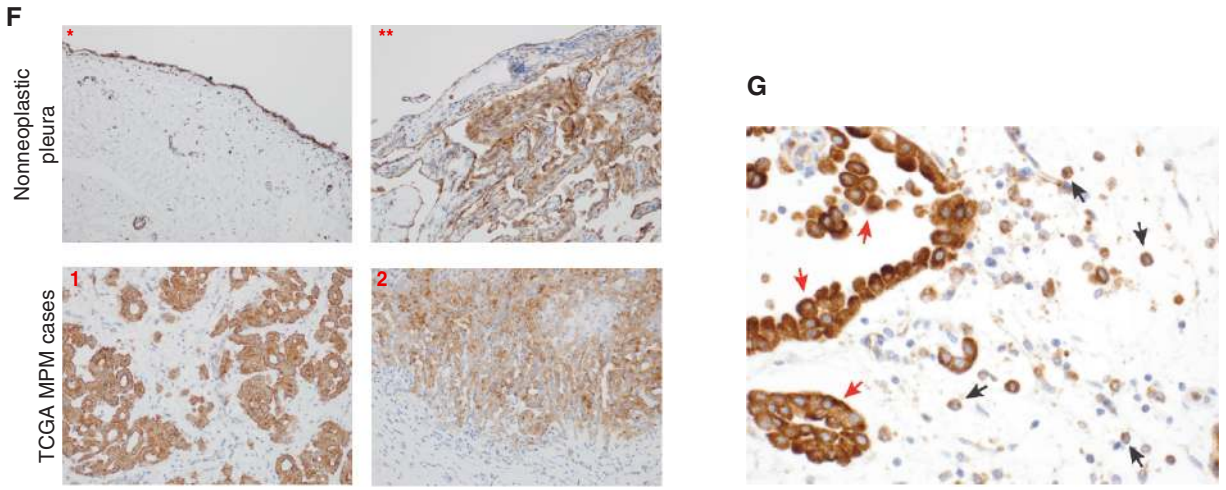

Figure 7. ***(Continued)*** **F,** IHC staining for VISTA (rabbit monoclonal anti-VISTA antibody, clone D1L2G, 0.1 μg/mL, Cell Signaling Technology) in normal mesothelial lining from pleura (*) and benign pleuritis with reactive mesothelial proliferation (**), and 2 TCGA MPM cases, TCGA-SC-A6LQ-01 (1) and TCGA-SC-A6LM-01 (2); images captured at 100× magnification. These results confirm high protein expression of VISTA on tumor cells in epithelioid MPM. **G,** VISTA immunohistochemistry. VISTA protein is expressed both in tumor cells (red arrows) and in infiltrating inflammatory cells (black arrows) in the epithelioid MPM case TCGA-SC-A6LQ-01. Image captured at 200× magnification.

expressed. Why chromosomes 5 and 7 are spared from the LOH in these MPM remains mysterious—interestingly, the same two chromosomes have recently been shown to also retain heterozygosity in thyroid Hürthle cell carcinomas with evidence of genomic near-haploidization (51). Overall, the identification of this novel subset of MPM highlights how, as the proportion of asbestos-related MPM plateaus and hopefully begins declining in Western countries, cases of possibly different etiology may become more apparent.

A better understanding of the determinants of aggressive behavior and predictors of poor clinical outcomes in MPM remains an unmet clinical need. To this end, integrative analyses with iCluster and PARADIGM revealed a set of molecular features that define MPM subsets with better and worse prognosis, and might point to candidate therapeutic targets. For instance, cases in the poor-prognosis subset showed higher *AURKA* mRNA expression, consistent with prior studies (14, 52). Treatment of MPM cell lines with an Aurora kinase inhibitor leads to growth arrest (53), and several Aurora kinase inhibitors are under investigation in patients with MPM. *AURKA* mRNA expression could be used to help identify patients with poor-prognosis epithelioid MPM so that they could be directed toward experimental therapies early in their treatment course. It is presently unclear whether Aurora kinase inhibitors will be active in MPM, and the ongoing phase II study of alisertib (NCT02293005) includes all patients irrespective of molecular signature. Although the value of targeting the AURKA pathway with currently available clinical compounds in MPM remains unknown, mRNA expression of *AURKA* is a prognostic marker that could be used in clinical practice to help stratify patients with epithelioid MPM.

Additionally, the poor-prognosis group also exhibited upregulation of the PI3K and mTOR signaling pathways. Preclinical studies have reported this finding, leading to clinical trials with a low response rate (2%) and no significant survival benefit in the salvage setting (54). These data suggest that combination therapies with mTOR inhibition may be necessary. Our analysis of epigenetic alterations revealed some associations between *BAP1* status and DNA methylation (Supplementary Table S6). A recently established functional link between BAP1 and EZH2 (22) provided the rationale for the recently completed clinical trial of the EZH2 inhibitor tazemetostat in *BAP1*-null MPM (NCT028602). By contrast, no relevant findings resulted from our analysis of viral and microbial sequences (Supplementary Table S7). Finally, another genomically driven potential vulnerability in MPM is very frequent *CDKN2A* deletion associated with codeletion of *MTAP,* the latter recently shown to metabolically lead to impaired activity, and therefore sensitization to further inhibition, of the arginine methyltransferase PRMT5 (12, 13), an inhibitor of which is currently being evaluated in a phase I trial (NCT02783300).

Harnessing current immunotherapy approaches to improve outcomes of patients with MPM is an area of intense clinical interest. Although our study confirms that MPMs show a low tumor mutation burden and therefore may present a more challenging setting for immunotherapy, a remarkable and novel finding of the present study is that of strong expression of the immune-checkpoint gene *VISTA* in epithelioid MPM, on the tumor cells themselves, unlike other cancer types where it is more often expressed on infiltrating reactive cells (42). VISTA is a member of the B7 family of negative checkpoint regulators that is expressed primarily on infiltrating tumor macrophages, and whose immune restraining effects on T cells may be similar to those of PD-1 (43, 55). However, unique structural features mean that VISTA can repress activation of T cells both as a ligand present on the surface of APC cells and as a receptor on the surface of T cells (56). Because VISTA is expressed on MPM cells, and its mRNA expression levels do not correlate with overall mutation

Downloaded from http://aacrjournals.org/cancerdiscovery/article-pdf/8/12/1548/1728852/1548.pdf by guest on 20 August 2022

load, our results raise the possibility that VISTA expression may be restraining antitumor immune responses in a subset of MPM cases. As we find that nonneoplastic mesothelium also expresses VISTA protein, we speculate that VISTA expression in MPM is retained or possibly selected for by immune pressure. This is consistent with previous publications demonstrating that MPM is an "immunogenic" tumor (57), including recent trials showing some responses to immune-checkpoint blockade therapy (58, 59). Indeed, VISTA has recently been reported as a possible compensatory immune-inhibitory pathway in prostate cancers that fail to respond to ipilimumab (60). Our findings thus provide both a rationale and a candidate biomarker for clinical trials of emerging anti-VISTA therapy (refs. 42, 44; NCT02812875) in epithelioid MPM. Taken together, our findings point to new lines of investigation into the biology of MPM with the potential to lead to new therapeutic strategies.

METHODS

TCGA Project Management has collected necessary human subjects documentation to ensure the project complies with 45-CFR-46 (the "Common Rule"). The program has obtained documentation from every contributing clinical site to verify that Institutional Review Board (IRB) approval has been obtained to participate in TCGA. Such documented approval may include one or more of the following:

- An IRB-approved protocol with informed consent specific to TCGA or a substantially similar program. In the latter case, if the protocol was not TCGA-specific, the clinical site principal investigator provided a further finding from the IRB that the already-approved protocol is sufficient to participate in TCGA.
- A TCGA-specific IRB waiver has been granted.
- A TCGA-specific letter that the IRB considers one of the exemptions in 45-CFR-46 applicable. The two most common exemptions cited were that the research falls under 46.102(f)(2) or 46.101(b)(4). Both exempt requirements for informed consent, because the received data and material do not contain directly identifiable private information.
- A TCGA-specific letter that the IRB does not consider the use of these data and materials to be human subjects research. This was most common for collections in which the donors were deceased.

A detailed description of the sample acquisition and pathology review process, as well as the experimental and computational methods used for the different analyses presented in our study, is provided as Supplementary Sections 1–13.

Disclosure of Potential Conflicts of Interest

L.R. Chirieac has received remuneration for medicolegal work related to mesothelioma. V.W. Rusch reports receiving a commercial research grant from Genentech and is a consultant/advisory board member for BMS. H. Pass reports receiving a commercial research grant from Genentech. M.G. Zauderer is a member of the Board of Directors of the Mesothelioma Applied Research Foundation, reports receiving commercial research grants from Bristol-Meyers Squibb and Millennium, and is a consultant/advisory board member for AstraZeneca, Sellas Life Science, and Epizyme. D.J. Kwiatkowski is a consultant/advisory board member for Novartis. R. Bueno has ownership interest (including stock, patents, etc.) in Navigation Sciences. A.D. Cherniack reports receiving commercial research support from Bayer. No potential conflicts of interest were disclosed by the other authors.

Authors' Contributions

Co-chairs: Marc Ladanyi, Peter J. Campbell, Bruce W. S. Robinson
Manuscript Coordinator: Julija Hmeljak
Analysis Coordinator: Ina Felau
Data Coordinator: Francisco Sanchez-Vega
Project Manager: Ina Felau
Copy-number: Andrew D. Cherniack, Juliann Shih
mRNA: Katherine A. Hoadley,
Methylation: Luda Danilova
miRNA: Reanne Bowlby, Gordon Robertson, Ewan Gibb
Exomes: Manaswi Gupta, Chip Stewart, Patrick Tarpey
RPPA: Rupa Kanchi, Rehan Akbani
Transcription factor analysis: Hatice U. Osmanbeyoglu

Integrative analyses:
PARADIGM: Yulia Newton, Kiley Graim,
Firehose: David Heiman, Michael Noble
iCluster: Esther Drill, Ronglai Shen; David T. Severson, Raphael Bueno
Regulome explorer: Lisa Iype, Vésteinn Thorsson, David L. Gibbs,
EMT analysis: Lauren A. Byers, Carl Gay, Lixia Dao

Tissue Source Sites: Michael Feldman, Harvey Pass, Nico van Zandwijk, Raphael Bueno, Anne Tsao, Marc Ladanyi, Robert Rintoul, Hedy Kindler, Rajiv Dhir, Bruce Robinson, Andre Carvalho, Troy Shelton
Pathology Subgroup: William D. Travis, Sanja Dacic, Lucian Chirieac, Françoise Galateau-Sallé, Junya Fujimoto, Aliya Husain, Marc Ladanyi
VISTA IHC: Patrice Desmeules, Achim Jungbluth
Clinical Subgroup: Marjorie Zauderer, Anne Tsao, David J. Kwiatkowski, Hedy Kindler, Harvey Pass, Jenette Creaney, Valerie Rusch, Robert C. Rintoul, Tara Lichtenberg, Bruce W. S. Robinson, Nathan Pennell, Henrique Silveira,
Genomic near-haploidization validation datasets: Gloria Ravegnini, Jonathan Fletcher, Hiroyuki Aburatani

The TCGA research network contributed collectively to this study. M.L., B.W.R.S. and P.J.C. oversaw data analyses and interpretation. J.H., F.S.-V., M.L., P.J.C., M.Z., R.S., B.W.S.R. and A.T. wrote the manuscript.

Acknowledgments

We thank Drs. Elaine Mardis and Matthew Meyerson for invaluable feedback and Dr. Lee Spraggon for helpful comments and assistance with figures. This work was supported by the following grants from the USA National Institutes of Health: U54 HG003273, U54 HG003067, U54 HG003079, U24 CA143799, U24 CA143835, U24 CA143840, U24 CA143843, U24 CA143845, U24 CA143848, U24 CA143858, U24 CA143866, U24 CA143867, U24 CA143882, U24 CA143883, U24 CA144025, P30 CA016672, and P30 CA008748. Whole-exome sequencing and analysis was funded by the British Lung Foundation grant APG11-7 ("The genomic architecture of mesothelioma"). Publication charges were funded by the Memorial Sloan Kettering Mesothelioma Program Fund.

The members of The Cancer Genome Atlas Research Network are Hiroyuki Aburatani, Rehan Akbani, Adrian Ally, Pavana Anur, Joshua Armenia, J. Todd Auman, Miruna Balasundaram, Saianand Balu, Stephen B. Baylin, Michael Becich, Carmen Behrens, Rameen Beroukhim, Craig Bielski, Tom Bodenheimer, Moiz S. Bootwalla, Jay Bowen, Reanne Bowlby, Denise Brooks, Raphael Bueno, Lauren Averett Byers, Flávio M. Cárcano, Rebecca Carlsen, Andre L. Carvalho, Andrew D. Cherniack, Dorothy Cheung, Lucian Chirieac, Juok Cho, Eric Chuah, Sudha Chudamani, Carrie Cibulskis, Leslie Cope, Daniel Crain, Jenette Creaney, Erin Curley, Sanja Dacic, Ludmila Danilova, Assunta De Rienzo, Timothy DeFreitas, John A. Demchok, Noreen Dhalla, Rajiv Dhir, Lixia Diao, Esther Drill, Ina Felau, Michael Feldman, Martin L. Ferguson, Jonathan A. Fletcher, Junya Fujimoto, Junya Fujimoto, Shiro Fukuda, Stacey B. Gabriel, Françoise Galateau Sallé, Jianjiong Gao, Johanna Gardner, Julie M. Gastier-Foster, Carl M. Gay, Nils Gehlenborg, Mark Gerken, Gad Getz, Ewan A. Gibb, David L. Gibbs, Chandra Goparaju, Kiley Graim, Benjamin Gross, Guangwu Guo, Manaswi Gupta, Seiki Hasegawa, David Haussler, D. Neil Hayes,

Downloaded from http://aacrjournals.org/cancerdiscovery/article-pdf/8/12/1548/1728852/1548.pdf by guest on 20 August 2022

David I. Heiman, Zachary Heins, Julija Hmeljak, Katherine A. Hoadley, Robert A. Holt, Alan P. Hoyle, Aliya Husain, Carolyn M. Hutter, Lisa Iype, Stuart R. Jefferys, Steven J.M. Jones, Corbin D. Jones, Rupa S. Kanchi, Katayoon Kasaian, Jaegil Kim, Hedy Kindler, Nobuyuki Kondo, Thomas Krausz, Ritika Kundra, Kozo Kuribayashi, David J. Kwiatkowski, Marc Ladanyi, Phillip H. Lai, Peter W. Laird, Michael S. Lawrence, Darlene Lee, Kristen M. Leraas, Tara M. Lichtenberg, Pei Lin, Jia Liu, Wenbin Liu, Eric Minwei Liu, Laxmi Lolla, Adhemar Longatto-Filho, Yiling Lu, James Luketich, Yussanne Ma, Dennis T. Maglinte, David Mallory, Marco A. Marra, Michael Mayo, Sam Meier, Jonathan Melamed, Shaowu Meng, Matthew Meyerson, Piotr A. Mieczkowski, Gordon B. Mills, Richard A. Moore, Cesar Moran, Scott Morris, Lisle E. Mose, Andrew J. Mungall, Karen Mungall, Takashi Nakano, Rashi Naresh, Yulia Newton, Michael S. Noble, Angelica Ochoa, Hatice Osmanbeyoglu, Joel S. Parker, Harvey I. Pass, Joseph Paulauskis, Arjun Pennathur, Nathan A. Pennell, Robert Penny, Charles M. Perou, Todd Pihl, Nilsa C. Ramirez, Doris M. Rassl, Gloria Ravegnini, Glen Reid, Rui M. Reis, Sheila M. Reynolds, David Rice, William G Richards, Robert C. Rintoul, Jeffrey Roach, A. Gordon Robertson, Valerie Rusch, Sara Sadeghi, Gordon Saksena, Francisco Sanchez-Vega, Chris Sander, Ayuko Sato, Cristovam Scapulatempo-Neto, Jacqueline E. Schein, Nikolaus Schultz, Steven E. Schumacher, Tanguy Seiwert, Yoshitaka Sekido, David T Severson, Candace Shelton, Troy Shelton, Ronglai Shen, Robert Sheridan, Yan Shi, Juliann Shih, Yuichi Shiraishi, Ilya Shmulevich, Henrique C. S. Silveira, Janae V. Simons, Payal Sipahimalani, Tara Skelly, Heidi J. Sofia, Matthew G. Soloway, Paul Spellman, Chip Stewart, Josh Stuart, Qiang Sun, Jumpei Takeshita, Angela Tam, Donghui Tan, Roy Tarnuzzer, Kenji Tatsuno, Barry S Taylor, Nina Thiessen, Eric Thompson, Vesteinn Thorsson, William D. Travis, Anne Tsao, Kane Tse, Tohru Tsujimura, Federico Valdivieso, David J. Van Den Berg, Nico van Zandwijk, Umadevi Veluvolu, Luciano S. Viana, Douglas Voet, Yunhu Wan, Zhining Wang, Jing Wang, Joellen Weaver, John N. Weinstein, Daniel J. Weisenberger, Matthew D. Wilkerson, Lisa Wise, Ignacio Wistuba, Tina Wong, Ye Wu, Shogo Yamamoto, Liming Yang, Marjorie G. Zauderer, Jean C. Zenklusen, Jiashan Zhang, Hailei Zhang, Hongxin Zhang, and Erik Zmuda.

Received July 17, 2018; revised September 6, 2018; accepted October 10, 2018; published first October 15, 2018.

REFERENCES

1. Sekido Y. Molecular pathogenesis of malignant mesothelioma. Carcinogenesis 2013;34:1413–9.
2. Leong SL, Zainudin R, Kazan-Allen L, Robinson BW. Asbestos in Asia. Respirology 2015;20:548–55.
3. Yap TA, Aerts JG, Popat S, Fennell DA. Novel insights into mesothelioma biology and implications for therapy. Nat Rev Cancer 2017;17:475–88.
4. Bott M, Brevet M, Taylor BS, Shimizu S, Ito T, Wang L, et al. The nuclear deubiquitinase BAP1 is commonly inactivated by somatic mutations and 3p21.1 losses in malignant pleural mesothelioma. Nat Genet 2011;43:668–72.
5. Bueno R, Stawiski EW, Goldstein LD, Durinck S, De Rienzo A, Modrusan Z, et al. Comprehensive genomic analysis of malignant pleural mesothelioma identifies recurrent mutations, gene fusions and splicing alterations. Nat Genet 2016;48:407–16.
6. Guo G, Chmielecki J, Goparaju C, Heguy A, Dolgalev I, Carbone M, et al. Whole-exome sequencing reveals frequent genetic alterations in BAP1, NF2, CDKN2A, and CUL1 in malignant pleural mesothelioma. Cancer Res 2015;75:264–9.
7. de Reynies A, Jaurand MC, Renier A, Couchy G, Hysi I, Elarouci N, et al. Molecular classification of malignant pleural mesothelioma: identification of a poor prognosis subgroup linked to the epithelial-to-mesenchymal transition. Clin Cancer Res 2014;20:1323–34.
8. Martincorena I, Campbell PJ. Somatic mutation in cancer and normal cells. Science 2015;349:1483–9.
9. Alexandrov LB, Jones PH, Wedge DC, Sale JE, Campbell PJ, Nik-Zainal S, et al. Clock-like mutational processes in human somatic cells. Nat Genet 2015;47:1402–7.
10. Chew SH, Toyokuni S. Malignant mesothelioma as an oxidative stress-induced cancer: an update. Free Radic Biol Med 2015;86:166–78.
11. Illei PB, Rusch VW, Zakowski MF, Ladanyi M. Homozygous deletion of CDKN2A and codeletion of the methylthioadenosine phosphorylase gene in the majority of pleural mesotheliomas. Clin Cancer Res 2003;9:2108–13.
12. Kryukov GV, Wilson FH, Ruth JR, Paulk J, Tsherniak A, Marlow SE, et al. MTAP deletion confers enhanced dependency on the PRMT5 arginine methyltransferase in cancer cells. Science 2016;351:1214–8.
13. Mavrakis KJ, McDonald ER 3rd, Schlabach MR, Billy E, Hoffman GR, deWeck A, et al. Disordered methionine metabolism in MTAP/CDKN2A-deleted cancers leads to dependence on PRMT5. Science 2016;351:1208–13.
14. Lopez-Rios F, Chuai S, Flores R, Shimizu S, Ohno T, Wakahara K, et al. Global gene expression profiling of pleural mesotheliomas: overexpression of aurora kinases and P16/CDKN2A deletion as prognostic factors and critical evaluation of microarray-based prognostic prediction. Cancer Res 2006;66:2970–9.
15. Dacic S, Kothmaier H, Land S, Shuai Y, Halbwedl I, Morbini P, et al. Prognostic significance of p16/cdkn2a loss in pleural malignant mesotheliomas. Virchows Arch 2008;453:627–35.
16. Panagopoulos I, Thorsen J, Gorunova L, Micci F, Haugom L, Davidson B, et al. RNA sequencing identifies fusion of the EWSR1 and YY1 genes in mesothelioma with t(14;22)(q32;q12). Genes Chromosomes Cancer 2013;52:733–40.
17. Desmeules P, Joubert P, Zhang L, Al-Ahmadie HA, Fletcher CD, Vakiani E, et al. A subset of malignant mesotheliomas in young adults are associated with recurrent EWSR1/FUS-ATF1 fusions. Am J Surg Pathol 2017;41:980–8.
18. Hung YP, Dong F, Watkins JC, Nardi V, Bueno R, Dal Cin P, et al. Identification of ALK rearrangements in malignant peritoneal mesothelioma. JAMA Oncol 2018;4:235–8.
19. Luchini C, Veronese N, Yachida S, Cheng L, Nottegar A, Stubbs B, et al. Different prognostic roles of tumor suppressor gene BAP1 in cancer: a systematic review with meta-analysis. Genes Chromosomes Cancer 2016;55:741–9.
20. Carbone M, Ferris LK, Baumann F, Napolitano A, Lum CA, Flores EG, et al. BAP1 cancer syndrome: malignant mesothelioma, uveal and cutaneous melanoma, and MBAITs. J Transl Med 2012;10:179.
21. Nasu M, Emi M, Pastorino S, Tanji M, Powers A, Luk H, et al. High Incidence of Somatic BAP1 alterations in sporadic malignant mesothelioma. J Thorac Oncol 2015;10:565–76.
22. LaFave LM, Beguelin W, Koche R, Teater M, Spitzer B, Chramiec A, et al. Loss of BAP1 function leads to EZH2-dependent transformation. Nat Med 2015;21:1344–9.
23. Osmanbeyoglu HU, Toska E, Chan C, Baselga J, Leslie CS. Pancancer modelling predicts the context-specific impact of somatic mutations on transcriptional programs. Nat Commun 2017;8:14249.
24. Yu H, Mashtalir N, Daou S, Hammond-Martel I, Ross J, Sui G, et al. The ubiquitin carboxyl hydrolase BAP1 forms a ternary complex with YY1 and HCF-1 and is a critical regulator of gene expression. Mol Cell Biol 2010;30:5071–85.
25. Boyd NH, Morgan JE, Greer SF. Polycomb recruitment at the Class II transactivator gene. Mol Immunol 2015;67(2 Pt B):482–91.
26. Broz ML, Binnewies M, Boldajipour B, Nelson AE, Pollack JL, Erle DJ, et al. Dissecting the tumor myeloid compartment reveals rare activating antigen-presenting cells critical for T cell immunity. Cancer Cell 2014;26:638–52.
27. Shen R, Seshan VE. FACETS: allele-specific copy number and clonal heterogeneity analysis tool for high-throughput DNA sequencing. Nucleic Acids Res 2016;44:e131.
28. Holmfeldt L, Wei L, Diaz-Flores E, Walsh M, Zhang J, Ding L, et al. The genomic landscape of hypodiploid acute lymphoblastic leukemia. Nat Genet 2013;45:242–52.
29. Zheng S, Cherniack AD, Dewal N, Moffitt RA, Danilova L, Murray BA, et al. Comprehensive pan-genomic characterization of adrenocortical carcinoma. Cancer Cell 2016;29:723–36.

Downloaded from http://aacrjournals.org/cancerdiscovery/article-pdf/8/12/1548/1728852/1548.pdf by guest on 20 August 2022

30. Nik-Zainal S, Van Loo P, Wedge DC, Alexandrov LB, Greenman CD, Lau KW, et al. The life history of 21 breast cancers. Cell 2012;149:994–1007.
31. Carter SL, Cibulskis K, Helman E, McKenna A, Shen H, Zack T, et al. Absolute quantification of somatic DNA alterations in human cancer. Nat Biotechnol 2012;30:413–21.
32. Shen R, Olshen AB, Ladanyi M. Integrative clustering of multiple genomic data types using a joint latent variable model with application to breast and lung cancer subtype analysis. Bioinformatics 2009;25:2906–12.
33. Vaske CJ, Benz SC, Sanborn JZ, Earl D, Szeto C, Zhu J, et al. Inference of patient-specific pathway activities from multi-dimensional cancer genomics data using PARADIGM. Bioinformatics 2010;26:i237–45.
34. Tan K, Kajino K, Momose S, Masaoka A, Sasahara K, Shiomi K, et al. Mesothelin (MSLN) promoter is hypomethylated in malignant mesothelioma, but its expression is not associated with methylation status of the promoter. Hum Pathol 2010;41:1330–8.
35. Williams M, Kirschner MB, Cheng YY, Hanh J, Weiss J, Mugridge N, et al. miR-193a-3p is a potential tumor suppressor in malignant pleural mesothelioma. Oncotarget 2015;6:23480–95.
36. Bindea G, Mlecnik B, Tosolini M, Kirilovsky A, Waldner M, Obenauf AC, et al. Spatiotemporal dynamics of intratumoral immune cells reveal the immune landscape in human cancer. Immunity 2013;39:782–95.
37. Maki Y, Nishimura Y, Toyooka S, Soh J, Tsukuda K, Shien K, et al. The proliferative effects of asbestos-exposed peripheral blood mononuclear cells on mesothelial cells. Oncol Lett 2016;11:3308–16.
38. Wright CM, Kirschner MB, Cheng YY, O'Byrne KJ, Gray SG, Schelch K, et al. Long non coding RNAs (lncRNAs) are dysregulated in malignant pleural mesothelioma (MPM). PLoS One 2013;8:e70940.
39. Renganathan A, Kresoja-Rakic J, Echeverry N, Ziltener G, Vrugt B, Opitz I, et al. GAS5 long non-coding RNA in malignant pleural mesothelioma. Mol Cancer 2014;13:119.
40. Mak MP, Tong P, Diao L, Cardnell RJ, Gibbons DL, William WN, et al. A patient-derived, pan-cancer EMT signature identifies global molecular alterations and immune target enrichment following epithelial-to-mesenchymal transition. Clin Cancer Res 2016;22:609–20.
41. Fassina A, Cappellesso R, Guzzardo V, Dalla Via L, Piccolo S, Ventura L, et al. Epithelial-mesenchymal transition in malignant mesothelioma. Mod Pathol 2012;25:86–99.
42. Lines JL, Sempere LF, Broughton T, Wang L, Noelle R. VISTA is a novel broad-spectrum negative checkpoint regulator for cancer immunotherapy. Cancer Immunol Res 2014;2:510–7.
43. Nowak EC, Lines JL, Varn FS, Deng J, Sarde A, Mabaera R, et al. Immunoregulatory functions of VISTA. Immunol Rev 2017;276:66–79.
44. Deng J, Le Mercier I, Kuta A, Noelle RJ. A new VISTA on combination therapy for negative checkpoint regulator blockade. J Immunother Cancer 2016;4:86.
45. Wang L, Rubinstein R, Lines JL, Wasiuk A, Ahonen C, Guo Y, et al. VISTA, a novel mouse Ig superfamily ligand that negatively regulates T cell responses. J Exp Med 2011;208:577–92.
46. Shaw TJ, Zhang XY, Huo Z, Robertson D, Lovell PA, Dalgleish AG, et al. Human peritoneal mesothelial cells display phagocytic and antigen-presenting functions to contribute to intraperitoneal immunity. Int J Gynecol Cancer 2016;26:833–8.
47. Mutti L, Valle MT, Balbi B, Orengo AM, Lazzaro A, Alciato P, et al. Primary human mesothelioma cells express class II MHC, ICAM-1 and B7-2 and can present recall antigens to autologous blood lymphocytes. Int J Cancer 1998;78:740–9.
48. Creaney J, Dick IM, Leon JS, Robinson BW. A proteomic analysis of the malignant mesothelioma secretome using iTRAQ. Cancer Genomics Proteomics 2017;14:103–17.
49. Kang HC, Kim HK, Lee S, Mendez P, Kim JW, Woodard G, et al. Whole exome and targeted deep sequencing identify genome-wide allelic loss and frequent SETDB1 mutations in malignant pleural mesotheliomas. Oncotarget 2016;7:8321–31.
50. Keniry A, Gearing LJ, Jansz N, Liu J, Holik AZ, Hickey PF, et al. Setdb1-mediated H3K9 methylation is enriched on the inactive X and plays a role in its epigenetic silencing. Epigenetics Chromatin 2016;9:16.
51. Ganly I, Makarov V, Deraje S, Dong Y, Reznik E, Seshan V, et al. Integrated genomic analysis of Hürthle Cell cancer reveals oncogenic drivers, recurrent mitochondrial mutations, and unique chromosomal landscapes. Cancer Cell 2018;34:256–270.e5.
52. Suraokar MB, Nunez MI, Diao L, Chow CW, Kim D, Behrens C, et al. Expression profiling stratifies mesothelioma tumors and signifies deregulation of spindle checkpoint pathway and microtubule network with therapeutic implications. Ann Oncol 2014;25:1184–92.
53. Crispi S, Fagliarone C, Biroccio A, D'Angelo C, Galati R, Sacchi A, et al. Antiproliferative effect of Aurora kinase targeting in mesothelioma. Lung Cancer 2010;70:271–9.
54. Ou SH, Moon J, Garland LL, Mack PC, Testa JR, Tsao AS, et al. SWOG S0722: phase II study of mTOR inhibitor everolimus (RAD001) in advanced malignant pleural mesothelioma (MPM). J Thorac Oncol 2015;10:387–91.
55. Liu J, Yuan Y, Chen W, Putra J, Suriawinata AA, Schenk AD, et al. Immune-checkpoint proteins VISTA and PD-1 nonredundantly regulate murine T-cell responses. Proc Natl Acad Sci U S A 2015;112:6682–7.
56. Flies DB, Han X, Higuchi T, Zheng L, Sun J, Ye JJ, et al. Coinhibitory receptor PD-1H preferentially suppresses CD4(+) T cell-mediated immunity. J Clin Invest 2014;124:1966–75.
57. Chee J, Robinson BW, Holt RA, Creaney J. Immunotherapy for lung malignancies: from gene sequencing to novel therapies. Chest 2017;151:891–7.
58. Alley EW, Lopez J, Santoro A, Morosky A, Saraf S, Piperdi B, et al. Clinical safety and activity of pembrolizumab in patients with malignant pleural mesothelioma (KEYNOTE-028): preliminary results from a non-randomised, open-label, phase 1b trial. Lancet Oncol 2017;18:623–30.
59. Scherpereel A, Mazieres J, Greillier L, Dô P, Bylicki O, Monnet I, et al. Second- or third-line nivolumab (Nivo) versus nivo plus ipilimumab (Ipi) in malignant pleural mesothelioma (MPM) patients: Results of the IFCT-1501 MAPS2 randomized phase II trial. J Clin Oncol 2017;35(18_suppl):LBA8507-LBA.
60. Gao J, Ward JF, Pettaway CA, Shi LZ, Subudhi SK, Vence LM, et al. VISTA is an inhibitory immune checkpoint that is increased after ipilimumab therapy in patients with prostate cancer. Nat Med 2017;23:551–5.

Downloaded from http://aacrjournals.org/cancerdiscovery/article-pdf/8/12/1548/1728852/1548.pdf by guest on 20 August 2022